HHS Public Access

Author manuscript

Nat Chem Biol. Author manuscript; available in PMC 2022 September 30.

Published in final edited form as:

Nat Chem Biol. 2022 July ; 18(7): 706–712. doi:10.1038/s41589-022-00994-9.

Structural basis for inhibition of the drug efflux pump NorA from *Staphylococcus aureus*

Douglas N. Brawley[1], **David B. Sauer**[1,+,#], **Jianping Li**[2,+], **Xuhui Zheng**[3,+], **Akiko Koide**[4,5,+], **Ganesh S. Jedhe**[2], **Tiffany Suwatthee**[2], **Jinmei Song**[1], **Zheng Liu**[6,#], **Paramjit S. Arora**[2], **Shohei Koide**[4,7,*], **Victor J. Torres**[3,8], **Da-Neng Wang**[1,9,*], **Nathaniel J. Traaseth**[2,*]

[1]Skirball Institute of Biomolecular Medicine, New York University School of Medicine, New York, NY, USA

[2]Department of Chemistry, New York University, New York, NY, USA

[3]Department of Microbiology, New York University School of Medicine, New York, New York, USA

[4]Perlmutter Cancer Center, New York University School of Medicine, New York, USA

[5]Department of Medicine, New York University School of Medicine, New York, USA

[6]Cryo-Electron Microscopy Facility, New York University School of Medicine, New York, NY, USA

[7]Department of Biochemistry and Molecular Pharmacology, New York University School of Medicine, New York, USA

[8]Antimicrobial-Resistant Pathogens Program, New York University School of Medicine, New York, USA.

[9]Department of Cell Biology, New York University School of Medicine, New York, NY, USA

[*]Corresponding authors: Shohei.Koide@nyulangone.org, da-neng.wang@med.nyu.edu, traaseth@nyu.edu.

[+]These authors contributed equally to this work

[#]Current addresses: D.B.S.: Centre for Medicines Discovery, Nuffield Department of Medicine, University of Oxford, Oxford, UKZ.L.: Kobilka Institute of Innovative Drug Discovery, School of Life and Health Sciences, The Chinese University of Hong Kong, Shenzhen, Guangdong 518172, China

Author Contributions

D.N.B. optimized NorA expression and purification protocols, screened Fabs, prepared samples for cryo-EM, performed binding assays, troubleshot cryoSPARC installation, processed and analyzed cryo-EM datasets, built atomic models, interpreted the structures, performed resistance assays of NorA mutations in *E. coli*, was involved in project design, and contributed to writing the manuscript. D.B.S. performed negative stain electron microscopy, froze grids for cryo-EM, processed and analyzed cryo-EM datasets, built atomic models, and interpreted the structures. J.L. performed the NorA-Fab inhibition experiment in *E. coli*, performed binding assays, carried out immunoblotting analyses, and prepared peptide stocks for MRSA inhibition experiments. X.Z. and V.J.T. designed and performed genetics, MIC, and growth inhibition experiments in MRSA and prepared membrane fractions from MRSA for immunoblotting analyses. A.K. and S.K. screened and identified Fabs that bind to NorA. G.S.J. and P.S.A. designed and generated peptides mimicking CDRH3. T.S. performed fluorescence polarization experiments with FITC-NPI-1 and the norfloxacin competition experiment. J.S. purified the membrane scaffold protein and performed NorA nanodisc reconstitution for Fab generation. Z.L. collected preliminary cryo-EM datasets. D.N.W. directed and designed the project and contributed to writing the manuscript. N.J.T. directed and designed the project and wrote the manuscript. All authors participated in data analysis and in revising the manuscript.

Competing Interest Declaration

S.K. is a SAB member and holds equity in and receives consulting fees from Black Diamond Therapeutics and receives research funding from Puretech Health and Argenx BVBA. V.J.T. is an inventor on patents and patent applications filed by NYU, which are currently under commercial license to Janssen Biotech Inc. Janssen Biotech Inc. provides research funding and other payments associated with the licensing agreement. All other authors declare no conflict of interest. NYU has filed a provisional patent application covering the NorA inhibitors described in this work.

Abstract

Membrane protein efflux pumps confer antibiotic resistance by extruding structurally distinct compounds and lowering their intracellular concentration. Yet there are no clinically approved drugs to inhibit efflux pumps, which would potentiate the efficacy of existing antibiotics rendered ineffective by drug efflux. Here we identified synthetic antigen-binding fragments (Fabs) that inhibit the quinolone transporter NorA from methicillin-resistant *Staphylococcus aureus* (MRSA). Structures of two NorA-Fab complexes determined using cryo-electron microscopy reveal a Fab loop deeply inserted in the substrate binding pocket of NorA. An arginine residue on this loop interacts with two neighboring aspartate and glutamate residues essential for NorA-mediated antibiotic resistance in MRSA. Peptide mimics of the Fab loop inhibit NorA with sub-micromolar potency and ablate MRSA growth in combination with the antibiotic norfloxacin. These findings establish a class of peptide inhibitors that block antibiotic efflux in MRSA by targeting indispensable residues in NorA without the need for membrane permeability.

Introduction

Widespread antibiotic resistance among hospital and community associated methicillin-resistant *Staphylococcus aureus* (MRSA), coupled with the lack of new antibiotics, poses an urgent threat to global public health[1]. Drug efflux is a first-line resistance mechanism used by MRSA to lower the intracellular antibiotic concentration[2–4], facilitating pathogen survival in the presence of antibiotics and the evolution of higher-level resistance mechanisms[3,5,6].

NorA is a chromosomally encoded multidrug efflux pump belonging to the core genome of *S. aureus* and present in all MRSA strains[7]. As a member of the major facilitator superfamily (MFS) and the DHA12 subfamily (12-transmembrane domain drug:H^+ antiporter), it couples drug extrusion to the proton motive force[8–10]. Overexpression of NorA through upregulating promoter mutations and/or chromosomal gene duplication[6,11,12] confers resistance to hydrophilic fluoroquinolones (ciprofloxacin, enoxacin, norfloxacin, ofloxacin), chloramphenicol, and cationic dyes[10,12–15]. This fitness advantage provided by NorA to *S. aureus* also allows for the evolution of mutations to the antibiotic target[6].

Despite NorA's biomedical relevance in *S. aureus* antibiotic resistance[9,10,12,14,15], there are no structural or functional data to explain the mechanisms underlying multidrug specificity or proton-coupled transport. Such information would provide key insight into the substrate binding pocket to aid in the design of potent and selective efflux pump inhibitors (EPIs). Combination treatments of EPIs with antibiotics are a promising therapeutic strategy for treating infections from pathogenic *S. aureus* strains and for reducing the emergence of higher-level resistance mechanisms[16,17]. However, development of EPIs has been hindered by systemic toxicity associated with off-target effects[18,19]. To date, there are no clinically approved inhibitors targeting efflux pumps in *S. aureus*.

Here, we set out to establish how NorA confers multidrug resistance to *S. aureus* by characterizing the transporter's structure, function, and mechanism using cryo-electron microscopy (cryo-EM) and *in vivo* drug resistance assays. In pursuing this goal, we

developed synthetic antigen-binding fragments (Fabs) that bind to the extracellular side of NorA and inhibit NorA-mediated antibiotic efflux.

Results

Structures of NorA-Fab complexes

To elucidate an atomic resolution structure of NorA (42 kDa) using single particle cryo-EM, we identified Fabs using phage display technology[20] that bound to NorA, which increased its effective mass to within the current limits of cryo-EM methodology[21,22]. Detergent-purified NorA was exchanged into amphipol and purified as a 1:1 complex with Fabs using size-exclusion chromatography (Extended Data Fig. 1a-c). Subsequent screening and cryo-EM data collection of NorA-Fab complexes revealed two suitable complexes for structure determination with K_d values of 1.2 ± 0.7 μM for NorA-Fab25 and 140 ± 20 nM for NorA-Fab36 (Extended Data Figs. 1d, 2, and 3a, b). Image processing of cryo-EM datasets generated Coulomb potential maps at resolutions of 3.74 Å for NorA-Fab25 and 3.16 Å for NorA-Fab36 (Extended Data Fig. 3c-h; Supplementary Table 1). While each map exhibited a minor preferred particle orientation and flexibility within the NorA-Fab complex (see Methods; Extended Data Fig. 3e-h; Supplementary Video 1, 2), these did not affect the interpretability of either map. As such, the quality of the maps was relatively uniform throughout each NorA-Fab complex and allowed for unambiguous chain tracing (Extended Data Figs. 3g, h and 4).

Both cryo-EM structures captured NorA in a similar outward-open conformation (1.2 Å RMSD) and in a 1:1 complex with each Fab (Fig. 1a, b; Extended Data Fig. 5a). NorA is comprised of 12-TM α-helices arranged in two 6-TM bundles (N- and C-terminal domains) that straddle a putative substrate binding pocket. The pocket is sealed from the cytoplasmic side of the membrane by interactions among TM4, TM5, TM10, and TM11 (Extended Data Fig. 5b). The N- and C-terminal domains interact through interdomain contacts between TM2-TM11 and TM5-TM8. These TM pairs display characteristic *hourglass* shapes, which likely facilitate conformational exchange through the *rocker-switch* mechanism[23–25]. Like other homologous DHA12 drug antiporters, NorA contains characteristic MFS sequence motifs, including Motif A and Motif C that are important for conformer stability and conformational exchange, respectively (Extended Data Fig. 5b)[26–28].

NorA's substrate binding pocket is largely hydrophobic (~65% lipophilic residues) and contains several aromatic residues, such as Phe16, Phe140, Phe303, and Phe306, which likely facilitate binding to aromatic drugs, including fluroquinolones[29]. The pocket also contains four ionizable residues (Arg98, Glu222, Asp307, Arg310) that create two distinct charged patches (Extended Data Fig. 5c). A positively charged patch is formed by Arg98 (TM4) in the N-terminal domain and a negatively charged patch is formed by neighboring residues Glu222 (TM7) and Asp307 (TM10) in the C-terminal domain which are proximal to Arg310 (TM10) (Fig. 1c, d; Fig. 2a). The acidic patch may play a functional role in drug binding as several substrates of NorA carry net positive charges[14].

NorA-Fab binding interfaces

Fab25 and Fab36 engage NorA from the extracellular side of the membrane through extensive intermolecular contacts. Most striking is the insertion of a hairpin loop, belonging to the heavy chain of CDR3 (CDRH3), into NorA's substrate binding pocket (Fig. 1c, d; Extended Data Fig. 6a-c). This aromatic-rich, 18-residue loop inserts ~15 Å into the pocket and interacts with NorA residues in the N- and C-terminal domains. Each CDRH3 loop contains a tryptophan-arginine motif, Trp133-Arg134, positioned at the tip and oriented for an intramolecular cation-π bond (Fig. 1c, d). On the opposite side of the arginine, the guanidinium group of Arg134 forms a second cation-π interaction with Phe303 (TM10) of NorA. This same arginine also makes electrostatic interactions with the carboxyl groups of Glu222 (TM7) and Asp307 (TM10) in NorA. In agreement with their importance in mediating contacts in the substrate binding pocket, mutation of the tryptophan (W133A) or arginine (R134A) in Fab36 CDRH3 resulted in ~20-fold and >100-fold reduced binding affinity to NorA (Extended Data Fig. 1e). Since Glu222 and Asp307 of NorA closely interact with Arg134 of each CDRH3 loop, these binding data also suggest the two acidic residues are critical for Fab binding.

Despite the similar mode of CDRH3 hairpin insertion for Fab25 and Fab36 into NorA's substrate binding pocket, we found three notable structural differences between the complexes. First, Fab25 and Fab36 bind NorA with distinct orientations that are rotated approximately 20° relative to one another along an axis orthogonal to the membrane plane (Fig. 1a, b). Second, the positions of CDRH3 loops between Fab25 and Fab36 are translated by ~5 Å relative to each other and interact with NorA differently. Namely, Trp133 of the tryptophan-arginine motif in Fab25 forms π-stacking interactions with Phe140 of NorA (Fig. 1c), while the indole nitrogen of Trp133 in Fab36 hydrogen bonds with the side chains of Asn137 and Asp307 of NorA (Fig. 1d). Third, Fab36 displays a more extensive binding surface with NorA (4,969 $Å^2$, sum of solvent-inaccessible surfaces) relative to the NorA-Fab25 interface (3,116 $Å^2$), which explains the ~9-fold tighter binding affinity (Extended Data Fig. 1d). A considerable portion of the additional Fab36 interaction surface is provided by an elongated lasso-shaped loop (Leu71 to Arg85 of the light chain) that traverses the upper portion of NorA's substrate binding pocket directly atop the CDRH3 hairpin loop (Extended Data Fig. 6d).

Key residues in NorA mediating drug resistance

To determine functionally important residues within NorA, we performed norfloxacin minimum inhibitory concentration (MIC) assays in a MRSA strain (USA300) where the native NorA gene was disrupted by a transposon insertion ($MRSA^{\Delta norA}$)[30]. Norfloxacin was found to elicit a bacteriostatic effect on the growth of MRSA and $MRSA^{\Delta norA}$ (Extended Data Fig. 7a). Wild-type NorA and 23 single-site mutations lining the substrate binding pocket were cloned into a hemin-inducible plasmid[31] and transformed into $MRSA^{\Delta norA}$. Expression of wild-type NorA conferred a 20-fold greater norfloxacin MIC relative to $MRSA^{\Delta norA}$ alone (Fig. 2b), underscoring NorA's functional role in mediating antibiotic resistance. From the panel of mutants, we identified 11 residues that displayed a 4-fold or greater reduction in MIC relative to wild-type NorA: Phe16, Gly20, and Ile23 in TM1; Asn137 and Phe140 in TM5; Glu222 in TM7; Q255 in TM8; Phe303, Phe306,

and Asp307 in TM10; Thr336 in TM11 (Fig. 2b). Each loss-of-function mutant was assessed for expression in MRSA$^{\Delta norA}$ to substantiate the functional significance of the MIC measurements (Extended Data Fig. 7b). When mapped onto the NorA structure, these residues outline a cluster within the substrate binding pocket that spans across the N- and C-terminal domains (Fig. 2c). Based on the spatial arrangement of these functionally important residues, we propose this cluster defines both the norfloxacin- and proton-binding sites in NorA. Overlapping binding sites are a mechanism used by some exchangers to facilitate antiport by preventing simultaneous proton and substrate binding[25,32]. Notably, among the 11 identified residues in NorA's substrate binding pocket, Asn137, Phe140, Glu222, Phe303, and Asp307 mediated intermolecular contacts with CDRH3 of Fab25 and/or Fab36 (Fig. 1c, d).

Within the putative drug/proton binding site is an anionic patch comprised of Glu222 and Asp307 (Fig. 2a). Substitution of either residue to alanine ablated NorA-mediated norfloxacin resistance in MRSA$^{\Delta norA}$ (Fig. 2b). To determine whether an ionizable carboxylate group was required for resistance at either position, we performed MIC and growth inhibition experiments in the presence of norfloxacin in MRSA$^{\Delta norA}$ using NorA mutants E222Q and D307N. MIC measurements for E222Q and D307N revealed ablated resistance phenotypes comparable to E222A and D307A, respectively (Fig. 2b). Similarly, growth inhibition assays in the presence of norfloxacin showed loss-of-function phenotypes for E222Q and D307N (Extended Data Fig. 7c). Together, these data indicate a functional role for Glu222 and Asp307 in proton-coupled transport.

Asp63 in TM2 is the third essential anionic residue in NorA, which was identified from MRSA$^{\Delta norA}$ and *E. coli* resistance assays with the D63A and D63N mutants (Extended Data Fig. 7c-e). However, unlike Glu222 and Asp307, Asp63 is not involved in proton transport due to its location outside of the membrane; instead, it is a conserved residue found within Motif A of MFS transporters that forms a hydrogen bond with the backbone amide hydrogen of Arg324 (TM11) to stabilize the outward-open conformation (Extended Data Fig. 5b)[27].

The NorA structures coupled with functional data strongly implicate Glu222 and Asp307 as the only negatively charged residues involved in the proton-coupling mechanism. These residues are conserved in NorA's closest homologues, Bmr and Blt from *B. subtilis*, yet are absent at corresponding positions in other DHA12 subfamily efflux pumps of known structure (EmrD, LmrP, MdfA, YajR[27,33–35]) (Fig. 2d). These efflux pumps instead contain essential aspartate and glutamate residues for proton-coupled transport at different membrane-embedded locations[27,36]. This observation highlights the subtle differences in transport mechanisms even among homologous drug efflux pumps.

Inhibition of NorA by Fabs

The insertion of Fab CDRH3 loops into the substrate binding pocket of NorA, as observed in the cryo-EM structures, immediately suggested Fab binding would inhibit antibiotic efflux (Fig. 1; Extended Data Fig. 8a). To test this hypothesis and avoid complications associated with Fab (50 kDa) permeation through the *S. aureus* peptidoglycan cell wall[37], we designed an inhibition experiment in *E. coli* where NorA and Fabs were co-expressed under the control of separate inducible promoters (Fig. 3a). Since NorA is located within

the inner membrane and confers norfloxacin resistance to *E. coli* (Extended Data Fig. 7d), we assessed growth inhibition by co-expressing Fabs in the periplasm to allow access to the extracellular face of NorA. Growth curves (OD_{600nm} vs. time) were quantified with or without norfloxacin and with variable concentrations of arabinose for inducing Fab expression. Co-expression of NorA with Fab36 in the presence of norfloxacin strongly attenuated *E. coli* growth in an arabinose-dependent manner (Fig. 3b-d). Similar experiments with Fab25 also showed inhibition of NorA, albeit to a lesser extent than for Fab36, which correlated with its poorer binding affinity to NorA (Extended Data Fig. 8b-e). In contrast, co-expression of NorA with a negative-control Fab ($Fab_{control}$), containing polyserine residues in the CDR loops, showed no inhibition (Fig. 3b-d). Likewise, we observed no growth inhibition for Fab25, Fab36, or $Fab_{control}$ in the absence of norfloxacin (Extended Data Fig. 8b, c), which supports a synergistic effect on *E. coli* growth attenuation only when both the Fab inhibitor and antibiotic are present.

To validate that NorA inhibition resulted from direct binding by the Fabs in *E. coli*, we carried out a pull-down experiment by co-expressing NorA with Fabs and purifying NorA from the membrane fraction. The elution fraction of NorA co-expressed with Fab25 and Fab36 contained the Fabs as detected through immunoblotting, while no Fab was detected in the elution of NorA co-expressed with $Fab_{control}$ (Extended Data Fig. 8f). Taken together with the growth inhibition results, these data confirm that Fab25 and Fab36 can bind and inhibit NorA in *E. coli*. Furthermore, since the $Fab_{control}$ was unable to bind or inhibit NorA, we conclude that the insertion of the CDRH3 loop into the substrate binding pocket of NorA, as observed in the cryo-EM structures, was responsible for the mode of inhibition.

CDRH3 peptides potentiate norfloxacin activity against MRSA

Inhibition of NorA by Fabs and the insertion of CDRH3 into the substrate binding pocket suggested that peptides mimicking the structure of the CDRH3 loops might also inhibit NorA. Such peptides would likely permeate the dense *S. aureus* peptidoglycan cell wall more efficiently than the 50-kDa Fabs[37]. Since Fab36 displayed better binding affinity and inhibition to NorA than Fab25, we synthesized a peptide (NorA peptide inhibitor, NPI-1) corresponding to a segment of Fab36 CDRH3 (Tyr128 to Trp139) with an additional C-terminal arginine residue for solubility (Fig. 4a; Extended Data Fig. 9a) and tested its ability to potentiate norfloxacin activity against MRSA. In the presence of norfloxacin, NPI-1 produced dose-dependent growth inhibition of MRSA with an IC_{50} value of 0.72 ± 0.08 μM (Fig. 4a, b). Notably, NPI-1 did not inhibit the growth of MRSA in the absence of norfloxacin, supporting the peptide's role as an adjuvant (Extended Data Fig. 9b). Furthermore, a control peptide substituting a glutamate for the arginine residue in the tryptophan-arginine motif (NPI-2) displayed no growth arrest of MRSA in the presence of norfloxacin (Fig. 4b, c; Extended Data Fig. 9c, d).

To validate interactions *in vitro*, we performed fluorescence polarization (FP) experiments and determined NPI-1 bound to NorA with a K_d value of 10 ± 5 nM (Fig. 4d). Additionally, we found that norfloxacin competes with NPI-1 binding to NorA, as revealed through a competition assay (Fig. 4e). Lastly, we determined that NPI-1 could displace bound Fab36 from NorA (Fig. 4f), in a manner consistent with NPI-1's K_d value to NorA. This result

supports the conclusion that NPI-1 makes similar intermolecular contacts as CDRH3 within the NorA-Fab36 complex. It is notable that NPI-1 bound NorA with ~14-fold greater affinity than Fab36 to NorA. We hypothesize this stems from NPI-1 retaining only the most critical interactions with NorA. Collectively, these data confirm NPI-1 binding to NorA *in vitro* and demonstrate that peptides targeting essential residues in NorA can serve as potent inhibitors of MRSA growth in combination with antibiotics (Fig. 4g).

Discussion

In this work, synthetic antibodies were leveraged to determine NorA-Fab structures by cryo-EM and to design a sub-micromolar inhibitor of NorA. The latter studies resulted in the creation and subsequent validation of a peptide EPI that targets a primary antibiotic resistance mechanism used by MRSA for evading fluoroquinolone antibiotics. We envision three advantages of peptide EPIs for treating MRSA infections in combination with existing antibiotics. First, peptide EPIs can be readily modified given the tractability of peptide chemistry, facilitating improvements in affinity and reductions in off-target effects; the latter of which has impeded the development of small molecule EPIs as therapeutics. Second, peptide EPIs can penetrate through the peptidoglycan cell wall and target the extracellular surface of efflux pumps without the need to cross the cell membrane, thereby bypassing complications associated with membrane permeability. Third, peptide EPIs are expected to be less susceptible to escape mutations given their capacity to form larger interaction interfaces with efflux pumps compared to small molecules. NPI-1, for example, makes extensive intermolecular contacts with residues in NorA's substrate binding pocket that are essential for efflux activity (Asn137, Phe140, Glu222, Asp307). Therefore, an escape mechanism to nullify NPI-1 binding and inhibition would likely require two or more simultaneous mutations at positions that do not impact drug efflux activity − an unlikely scenario. For these reasons, the peptide EPI described in this work is a promising lead compound for treating MRSA infections in combination with fluoroquinolone antibiotics, which have previously been classified as ineffective due to resistance mechanisms mediated by NorA. To further validate NPI-1 and similar peptide EPIs as viable pre-clinical therapeutic candidates, additional work is needed to determine and optimize their mammalian toxicity profiles and susceptibility to host proteases. The latter will likely necessitate the use of higher stability peptidomimetics such as constrained β-hairpins[38]. Overcoming these immediate hurdles would establish peptide EPIs as a promising class of therapeutics for combatting antibiotic-resistant bacterial infections where current antibiotics are rendered ineffective due to drug efflux.

Methods

NorA expression and purification

The *S. aureus* NorA sequence (Uniprot accession code Q5HHX4) was cloned into a pET28 vector (Novagen) with a carboxy-terminal decahistidine tag. The construct was transformed into C43 (DE3) *E. coli* and expressed using the autoinduction method[39] with minor modifications[40]. Briefly, cells were grown at 32 °C in ZYP-5052 media supplemented with 1 mM $MgSO_4$. At an OD_{600nm} of 0.5, the temperature was reduced to 20 °C and

cultures were grown for an additional 18–20 hr. Cells were harvested by centrifugation and stored at −80 °C.

Cell pellets were resuspended and lysed in 40 mM Tris pH 8.0, 400 mM NaCl, and 10% glycerol and the resultant lysate was clarified by centrifugation. The membrane fraction was harvested by centrifuging for 3 hr at 35,000 RPM using a Beckman ultracentrifugation equipped with a Type 45 Ti fixed-angle rotor. Membranes were resuspended in 20 mM Tris pH 8.0, 300 mM NaCl, 10% glycerol, and 10 mM imidazole and solubilized with 1% (w/v) lauryl maltose neopentyl glycol (LMNG, Anatrace). NorA was purified using immobilized metal-affinity chromatography (IMAC). In brief, NorA was bound to cobalt affinity resin (ThermoFisher Scientific) and successively washed with IMAC Buffer (20 mM Tris pH 8.0, 200 mM NaCl, 10% glycerol, and 0.2 % (w/v) LMNG) containing 25 mM and 50 mM imidazole and eluted with 400 mM imidazole. NorA eluate fractions were dialyzed into size exclusion chromatography (SEC) buffer (20 mM Tris pH 7.5 and 100 mM NaCl) and incubated overnight with PMAL-C8 amphipol (Anatrace). For cryo-EM, the sample was incubated with Bio-beads (Bio-Rad) and subsequently purified on a Superdex 200 column (GE healthcare) equilibrated in SEC buffer. Peak fractions were pooled, concentrated with a 10 kDa centrifugal concentrator (Millipore), and used immediately or flash frozen and stored at −80 °C. For Fab screening, LMNG-purified NorA was reconstituted into lipid nanodiscs using MSP1E3D1 following a published protocol[41] and the efficiency of the reconstitution was examined by SDS-PAGE and negative stain electron microscopy.

Generation of synthetic Fabs

Sorting of an antibody phage-display library using nanodisc-embedded NorA prepared as described above was performed as previously described[42,43] with slight modifications. In each round, phage solution in 50 mM Tris-HCl pH 7.5, 100 mM NaCl, 1% BSA, and 0.1 mM TCEP was first incubated with 4 μM biotinylated nanodiscs loaded with lipid but without NorA (“empty nanodiscs”) complexed with streptavidin-coated magnetic beads (catalog number Z5481, Promega). Unbound phage particles were recovered and then incubated with 100 nM NorA in biotinylated nanodiscs in solution, and phages bound to NorA were mixed with streptavidin-coated magnetic beads. Using a Kingfisher instrument (Thermo Fisher), the beads were captured, washed in the same buffer for a total of five times, then the bound phages were eluted in 100 mM glycine-HCl (pH 2.2). The elution solution was immediately neutralized with 2 M Tris-HCl (pH 8.0). A total of four rounds of library sorting were performed. Enriched clones were individually tested using phage ELISA using nanodisc-embedded NorA and empty nanodiscs immobilized in the wells of 96-well Maxisorp plates precoated with streptavidin as described previously[42,44].

Fab expression and purification

Fabs were subcloned into a modified pTac expression vector[45] and subsequently rigidified in the hinge-region of the heavy-chain[46] by site-directed mutagenesis. A negative-control Fab ($Fab_{control}$) construct comprised of undifferentiated, polyserine CDR sequences was not rigidified and contained a C-terminal Avi–tag on the heavy chain. Each Fab was transformed into the 55244 strain of *E. coli* (ATCC) and expressed in TBG media for 22 hr at 30 °C. Cell pellets were harvested by centrifugation and resuspended in running buffer (20 mM sodium

phosphate pH 7.0) supplemented with 1 mg ml^{-1} hen egg lysozyme (Sigma). After cell lysis and the removal of cell debris by centrifugation, the supernatant was loaded onto a protein G column (GE Healthcare) equilibrated in running buffer. Following elution from the column with 100 mM glycine (pH 2.7), the Fabs samples were immediately neutralized with 2 M Tris buffer (pH 8). Peak fractions were pooled, flash-frozen, and stored at −80 °C until use.

Microscale thermophoresis binding assays

Amphipol-purified NorA underwent an additional round of SEC to remove free amphipol. Purified Fabs were prepared as described above and labelled with a primary amine-reactive 647 nm fluorophore (Nanotemper) according to the manufacturer's instructions. Efficient labelling was verified spectroscopically by measuring absorbance at 280 and 650 nm. Microscale thermophoresis (MST) experiments were performed on a Monolith NT.115 Pico instrument (Nanotemper Technologies). Labelled Fab at 40 nM final concentration was mixed with NorA in 20 mM Tris pH 7.0, 100 mM NaCl, and 0.025% (w/v) Tween-20. All samples were incubated for 15 min and loaded into premium glass capillaries. The normalized fluorescent signal (F_{norm}) was plotted as a function of ligand concentration and fit with a non-linear sigmoidal regression model (GraphPad Prism) using a Hill slope equal to 1.0 to obtain the K_d values. The error in K_d values for Fab25 (1.2 ± 0.7 μM) and Fab36 (140 ± 20 nM) represent the average and standard deviation of two independent runs with three replicates per independent run. The error range in the K_d value for $Fab36^{W133A}$ (2 to 4 μM) corresponds to the 95% confidence interval of the non-linear fit. The $Fab36^{R134A}$ binding curve could not be accurately fit and the K_d value was estimated to be greater than the highest concentration of NorA in the experiment (> 14 μM). MST binding experiments with $Fab36^{W133A}$ and $Fab36^{R134A}$ were collected with three replicates each.

Competitive peptide binding experiments were performed with MST using fluorescently labelled Fab36 as described above. These experiments used fixed concentrations of NorA in PMAL-C8 amphipol at 6 μM and Fab36 at 40 nM, and a variable concentration of NPI-1 from 1.5 nM to 50 μM. Competitive peptide binding experiments were collected with three replicates. The superimposed solid line on the competition MST dataset was calculated using an EC_{50} value at 6.286 mM determined from the FITC-NPI-1 binding constant to NorA[47,48] (see Fluorescence polarization experiments section below).

Cryo-EM sample preparation and data collection

NorA-Fab25 and NorA-Fab36 complexes were prepared identically. Amphipol-purified NorA was incubated with purified Fabs at a 1:3 molar ratio for 2 hr at 4 °C and then purified further using a Superdex 200 10/300 column in SEC buffer. Formation of the NorA-Fab complexes was confirmed using SDS-PAGE and negative stain electron microscopy. Cryo-EM grids were prepared by applying 3 μL of sample at ~2 mg mL^{-1} to glow-discharged QuantiAuFoil 300-mesh R1.2/1.3 grids (Quantifoil)[41,49]. The samples were blotted for 3.5 or 4 seconds under 100% humidity at 4 ºC before plunge-freezing into liquid ethane using a Mark IV Vitrobot (FEI).

Cryo-EM data for NorA-Fab25 and NorA-Fab36 samples were acquired on a Titan Krios microscope (FEI) equipped with a K3 direct electron detector (Gatan), using a GIF-Quantum

energy filter with a 20 eV slit width[41,49]. SerialEM[50] was used for automated data collection. Movies were collected at a nominal magnification of 81,000 x in SuperRes mode with a physical pixel size of 1.079 Å and dose-fractioned over 60 frames. The NorA-Fab25 and NorA-Fab36 datasets received an accumulated dose of 49 and 55.54 e^{-} $Å^{-2}$, respectively. A total of 3,102 movies were collected for NorA-Fab25 and 2,816 movies collected for NorA-Fab36.

Cryo-EM image processing and map analysis

The NorA-Fab25 and NorA-Fab36 datasets were processed in cryoSPARC[51] with identical methodologies[41,49]. Imported movies were motion corrected and CTF estimated, and micrographs with an overall resolution worse than 8 Å were excluded from subsequent analysis. Initial 2D class averages were generated using particles picked with an ellipse-based template. 2D classes representing NorA-Fab complexes were then used as templates for a second round of particle picking. A total of 4.1 and 3.73 million particles were selected from the NorA-Fab25 and NorA-Fab36 datasets, respectively. Particles underlying well-resolved 2D classes were used for initial *ab initio* model building, and all picked particles were used for the subsequent heterogenous 3D refinement. Particles from classes of the complete NorA-Fab complexes or NorA-Fab complexes apparently lacking the Fab constant domain were retained for subsequent rounds of *ab initio* model building and heterogeneous 3D classification. After multiple rounds, a non-uniform 3D refinement step was used to generate final 3.74 Å and 3.16 Å maps for NorA-Fab25 and NorA-Fab36, respectively, as assessed using the gold standard Fourier shell correlation (FSC). Final maps were sharpened using Phenix.auto_sharpen[52] for 3D model building.

The source of directional streaking in each NorA-Fab map was investigated by determining directional FSC curves[53], calculating new maps in cisTEM[54], and performing 3D variability analysis (3DVA) in cryoSPARC. The directional FSC distribution revealed a minor preferred orientation bias for both NorA-Fab complexes, consistent with the preferred particle orientations shown in the angular particle distribution heatmaps. The preferred orientation was more evident in the NorA-Fab36 complex. Following the strategy of Dang *et al.*[55] to examine the effect of preferred orientation on reconstruction quality, maps were also calculated in cisTEM for the NorA-Fab complexes. For each complex, the cisTEM and cryoSPARC maps were of similar overall resolution, sphericity, and map quality. 3DVA calculations were performed using 4.0 Å-filtered final maps from cryoSPARC and visualized as movies in Chimera[56]. In each NorA-Fab complex, a bending movement was observed at the NorA-Fab interface and the interdomain hinge-region between the variable and constant domains of the Fab. This movement was more pronounced in the NorA-Fab36 complex. Overall, this analysis revealed the directional streaking to be caused by a minor orientation bias and flexibility within the NorA-Fab complex; however, this imperfection in map quality did not influence the interpretability of the maps.

Building of structural models

The NorA-Fab complex structural models were built in Coot[57] and refined using Phenix[52]. Backbone N- and C-terminal domain structures of LacY (PDB ID: 2CFP) and MdfA (PDB ID: 6GV1) were used as references for NorA model building. The Fab for each complex was

rebuilt from a homologous Fab structure (PDB ID: 5E08) after removing the variable loop regions.

MIC assays in MRSA

Wild-type USA300 strain JE2 ("MRSA")[30] and isogenic strains, *norA::bursa* (MRSA$^{\Delta norA}$) containing empty vector, or hemin-inducible NorA variants were grown overnight at 37 °C in TSB media supplemented with 10 μg/ml chloramphenicol and 1 μM hemin. The cultures were diluted to approximately 1×10^8 CFU/ml and evenly spread on TSA plates supplemented with 5 μg/ml chloramphenicol and 1 μM hemin. The norfloxacin MIC test strips (Liofilchem) were placed in the center of the plate and the plates were incubated for 24 hr at 37 °C. The MIC values were read at the intersection of the inhibition eclipse and the strip. At least two independent MIC experiments were acquired for each sample; reported errors reflect the standard deviation among independent experiments.

Bacteriostatic/bactericidal effect of norfloxacin on MRSA

MRSA or MRSA$^{\Delta norA}$ were cultured overnight in 5 ml TSB and diluted 1:1,000 with TSB the next morning. In a round-bottom 96-well plate, 50 μl of the diluted culture was mixed with 50 μl of TSB supplemented with norfloxacin. The final concentration of MRSA or MRSA$^{\Delta norA}$ was ~1×10^6 CFU/ml and norfloxacin was 0, 12.5, or 25 μg/ml. The plate was incubated while shaking at 37 °C. At 0 hr and after 1, 2, or 4 hr of incubation, CFUs of MRSA or MRSA$^{\Delta norA}$ were enumerated by serially diluting in PBS and spot plating on TSA plates.

Growth inhibition assays in MRSA

Wild-type MRSA and MRSA$^{\Delta norA}$ containing empty vector or hemin-inducible NorA variants were grown overnight at 37 °C in TSB media supplemented with 10 μg/ml chloramphenicol. The cultures were diluted 1:1,000 in TSB supplemented with 5 μg/ml chloramphenicol and 1 μM hemin, in the presence or the absence of norfloxacin (12.5 μg/ml). OD_{600nm} was measured as a function of time in a BioScreen C device at 37 °C with shaking between measurements every 15 min. At least two independent experiments were acquired with two technical replicates per experiment for each sample; reported errors reflect the standard deviation among technical replicates in a representative experiment.

To test the effects of peptides, overnight cultures of wild-type MRSA and MRSA$^{\Delta norA}$ in TSB media were diluted 1:1,000 in TSB with varying concentrations of peptides, in the presence or the absence of norfloxacin (12.5 μg/ml). All the peptide concentrations contained equal amount of the DMSO vehicle. OD_{600nm} was measured as a function of time in a BioScreen C device at 37 °C with shaking between measurements every 15 min. Three independent experiments were acquired; reported errors reflect the standard deviation among the independent experiments.

Characterization of NorA and mutant expression levels in MRSA

MRSA$^{\Delta norA}$ containing empty vector or hemin-inducible NorA variants were grown overnight at 37 °C in TSB media supplemented with 5 μg/ml chloramphenicol and 2.5 μM hemin. MRSA cell pellets were lysed in 40 μg/ml lysostaphin, 20 u/ml DNase, 40

μg/ml RNase A, 1x Halt Protease Inhibitor Cocktail in 50 mM Tris pH 7.5, 10 mM $MgCl_2$, and 1 mM $CaCl_2$ in Lysing matrix B tubes and bead beat for 3 rounds at 6 m/s. After removing the cell debris by centrifuging for 10 min at 10,000 RPM in an Eppendorf 5430 R microcentrifuge, the membrane fractions were pelleted from the supernatant by centrifuging for 1 hr at 40,000 RPM in a Beckman Optima MAX-TL ultracentrifuge equipped with a TLA-100 rotor. The membrane fractions were solubilized with a solution containing 2% SDS, 1x Halt Protease Inhibitor Cocktail, and 50 mM Tris pH 6.8. Protein concentrations were determined by a BCA assay. Total protein for each sample was normalized and subsequently loaded on the SDS-PAGE gel and immunoblotted using primary antibodies to the C-terminal myc tag on NorA (Genscript) and SrtA[58] using dilutions of 1:1,000 and 1:20,000, respectively.

NorA resistance assays in E. coli

Wild-type NorA harboring a C-terminal myc-tag in pTrcHis2C (Invitrogen)[9] was used to engineer NorA mutants using site-directed mutagenesis. Wild-type NorA, NorA mutants, or empty vector were transformed into BL21 DE3 *E. coli* and grown at 37 °C in LB media. At an OD_{600nm} of 1.0, the cultures were spotted in 10-fold serial dilutions on LB-agar plates infused with norfloxacin (15 nM). After overnight incubation at 37 °C, plates were imaged using a gel documentation system (Bio-Rad). The serial dilution screen was performed one time; loss-of-function mutants identified from the screen were confirmed in independent *E. coli* serial dilution experiments and in $MRSA^{\Delta norA}$ using MIC and growth inhibition experiments (see above).

Inhibition of NorA by Fabs in E. coli

NorA was encoded in a pTrcHis2C plasmid (ampicillin resistance) with a C-terminal myc-tag[9], while Fabs were cloned in a pBAD33 plasmid (gentamicin resistance)[59] with a C-terminal Avi-tag on the heavy chain of the Fab. Competent Top10 *E. coli* were co-transformed with vectors containing NorA and Fabs (Fab25, Fab36, or $Fab_{control}$) and grown on LB agar plates infused with carbenicillin and gentamicin. For time dependent growth curves, a single colony from the transformation was inoculated into TBG media in the presence of carbenicillin and gentamicin. The culture was grown to saturation for ~20 hr at 30 °C. Cultures were diluted by 300-fold into fresh TBG media containing carbenicillin and gentamicin, norfloxacin (0 or 1.2 μg/ml), and arabinose (0%, 0.0001%, 0.0005%, 0.0025%, 0.01%, 0.05%, 0.1%, 0.2%, 0.4%, or 0.8%). OD_{600nm} was measured as a function of time in a BioScreen Pro C device at 30 °C with shaking between measurements every 15 min. Four independent experiments were acquired with two technical replicates per experiment; reported errors reflect the standard deviation among the experiments.

Immunoblot (IB) analyses were performed on *E. coli* lysates co-expressing NorA and Fabs following 24 hr of growth in TBG media in the absence of norfloxacin. Primary antibodies at 1:1,000 dilutions detected the C-terminal myc tag on NorA (Genscript) and the C-terminal Avi tag on the heavy chain of the Fab (Genscript). IB analyses were repeated two independent times.

Synthesis of peptides mimicking Fab36 CDRH3

Peptides NPI-1 (NH_2-YYYYAWRVGGYWR-$CONH_2$) and NPI-2 (NH_2-YYYYAWEVGGYWR-$CONH_2$) were synthesized on Gyros Protein Technologies PurePep Chorus automated peptide synthesizer using standard Fmoc peptide synthesis on Rink amide resin (0.27 mmol/g). A fluorescent analog of NPI-1 (FITC-NPI-1: FITC-βA-YYYYAWRVGGYWR-$CONH_2$) was also synthesized by treating resin-bound NPI-1 with fluorescein isothiocyanate (1.25 eq.) and DIEA (2.5 eq.) in DMF for 2 hr. Synthesized peptides were globally deprotected and cleaved from resin with reagent K (82.5% TFA, 5% water, 5% phenol, 5% thioanisole, and 2.5% 1,2-ethanedithiol) for 2 hr. The mixture was concentrated, and the peptides were precipitated with diethyl ether. Peptides were purified by reverse-phase HPLC using a preparative-scale C18 column. Purity of the peptides was confirmed by analytical HPLC. Purified peptides were characterized by MALDI-TOF mass spectrometry. NPI-1: observed mass of 1802.05 $[M+H]^+$; calculated mass of 1801.85 $[M+H]^+$. NPI-2: observed mass of 1775.07 $[M+H]^+$; calculated mass of 1774.79 $[M+H]^+$. FITC-NPI-1: observed mass of 2263.76 $[M+H]^+$; calculated mass of 2263.95 $[M+H]^+$.

Fluorescence polarization experiments

Amphipol-purified NorA underwent an additional round of SEC to remove free amphipol. Fluorescence polarization (FP) experiments were performed on a DTX 880 Multimode Detector (Beckman) at 25 °C with excitation and emission wavelengths set to 485 and 525 nm, respectively. For NorA binding assays, increasing concentrations of NorA were added to wells of 15 nM FITC-NPI-1 in 100 μL solutions of 20 mM Tris pH 7.5, 100 mM NaCl, 10% glycerol, 0.1% pluronic acid, and 1.2% DMSO on black, U-shape 96 well plates (BRAND*plates*). All samples were incubated for 15 min on a shaking plate. FP values as a function of NorA concentration ($[L]$) were fit using the following quadratic binding equation in GraphPad Prism to obtain the binding affinity (K_d) for FITC-NPI-1 ($[P]_T$).

$$FP = \frac{K_d + [L] + [P]_T - \sqrt{(K_d + [L] + [P]_T)^2 - 4[L][P]_T}}{2[L][P]_T} Y_{\max} + Y_{\text{offset}}$$

$Y_{\max}$ and Y_{offset} are normalization parameters. The reported K_d value and error for FITC-NPI-1 reflects the average and standard deviation among seven independent experiments, each performed in triplicate.

FP competition binding experiments with norfloxacin were performed using FITC-NPI-1 as described above. These experiments used a fixed concentration of NorA in PMAL-C8 amphipol at 50 nM and FITC-NPI-1 at 15 nM with norfloxacin concentrations of 10 nM and 2 mM in 100 μL solutions of 20 mM Tris pH 7.5, 100 mM NaCl, 10% glycerol, 0.1% pluronic acid, and 1.2% DMSO. A control experiment was performed in the same manner but in the absence of NorA. Four independent trials of FP experiments were performed, each in triplicate.

Data Availability

The datasets generated during and/or analyzed during the current study are deposited in the Electron Microscopy Data Bank and Protein Data Bank for NorA-Fab25 (EMD-23463, PDB ID: 7LO7) and NorA-Fab36 (EMD-23464, PDB ID: 7LO8). Other data generated in this study are included in source data files.

Additional Information

Supplementary Information is available for this paper. Correspondence and requests for materials should be addressed to traaseth@nyu.edu, da-neng.wang@med.nyu.edu, or Shohei.Koide@nyulangone.org.

Extended Data

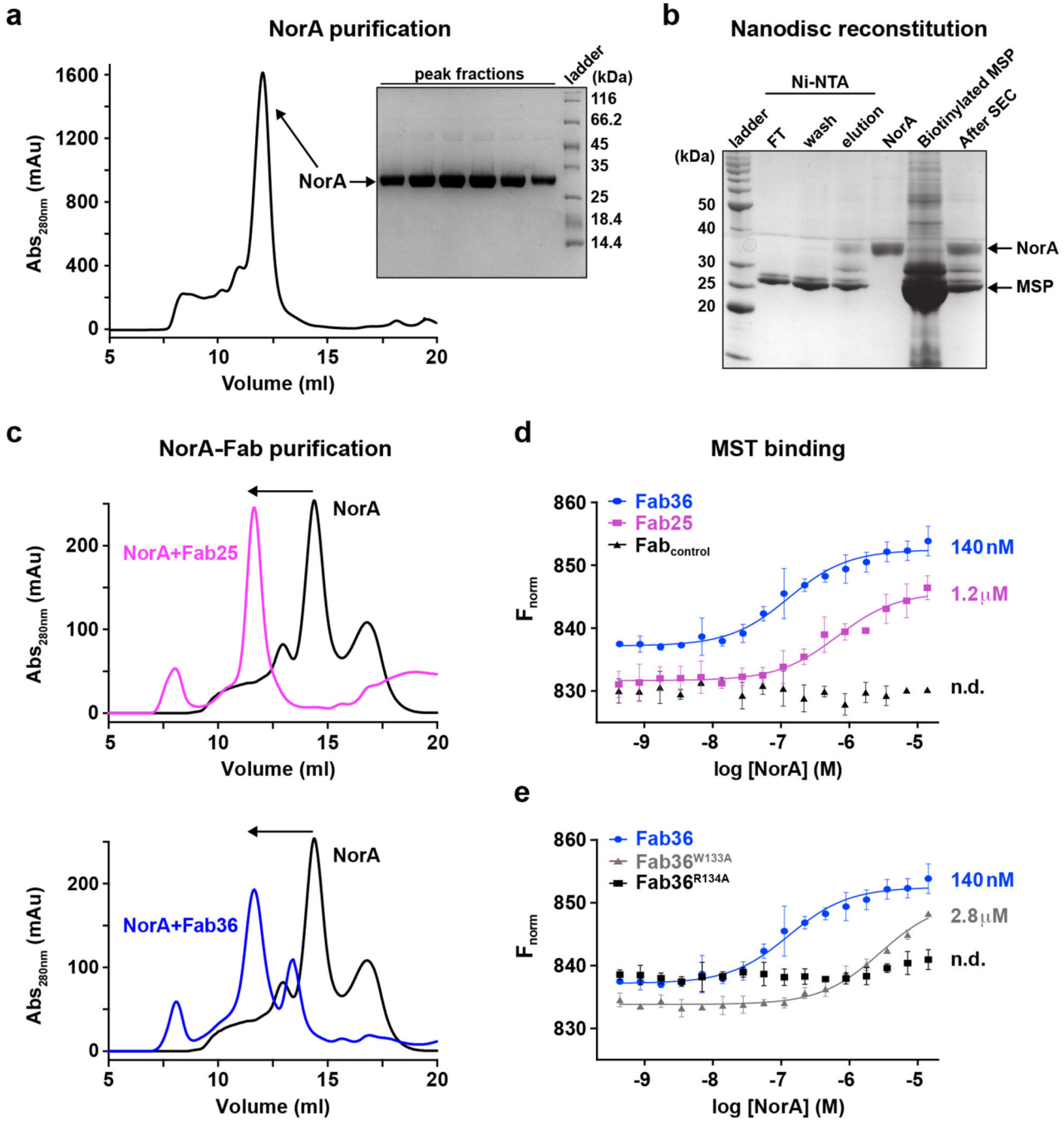

Extended Data Fig. 1. Preparation of NorA samples for Fab screening and cryo-EM.

a. Purification of NorA in LMNG detergent. Left: SEC chromatogram displaying absorbance at 280 nm (Abs_{280nm}) for NorA in LMNG. Right: Coomassie-stained SDS-PAGE gel of the SEC chromatogram. Similar results were obtained in ~15 independent experiments.

b. Coomassie-stained SDS-PAGE gel showing successful reconstitution of NorA (His-tagged) into biotinylated membrane scaffold protein (MSP) nanodiscs for phage display screening of Fabs. The sample was passed over a Ni-NTA column with the imidazole elution displaying both NorA and MSP bands. Similar reconstitution results were obtained in three independent experiments.

c. SEC chromatograms of NorA in PMAL-C8 amphipol alone and NorA in the presence of three-fold molar excess of Fab25 (top) or Fab36 (bottom). Major fractions from the left-shifted peaks indicated by arrows were collected and applied onto cryo-EM grids for structure determination.

d, e. MST binding curves of fluorescently labelled Fabs to NorA reconstituted in PMAL-C8 amphipol. K_d values are shown next to each dataset; "n.d." refers to not determined. The error in K_d values for Fab25 (1.2 ± 0.7 μM) and Fab36 (140 ± 20 nM) represent the average and standard deviation of two independent runs with three or four replicates per independent run. The error range in the K_d value for Fab36^{W133A} (2 to 4 μM) corresponds to the 95% confidence interval of the non-linear fit. The Fab36^{R134A} binding curve could not be accurately fit and the K_d value was estimated to be greater than the highest concentration of NorA in the experiment (> 14 μM). MST binding experiments with Fab36^{W133A} and Fab36^{R134A} were collected with three replicates each.

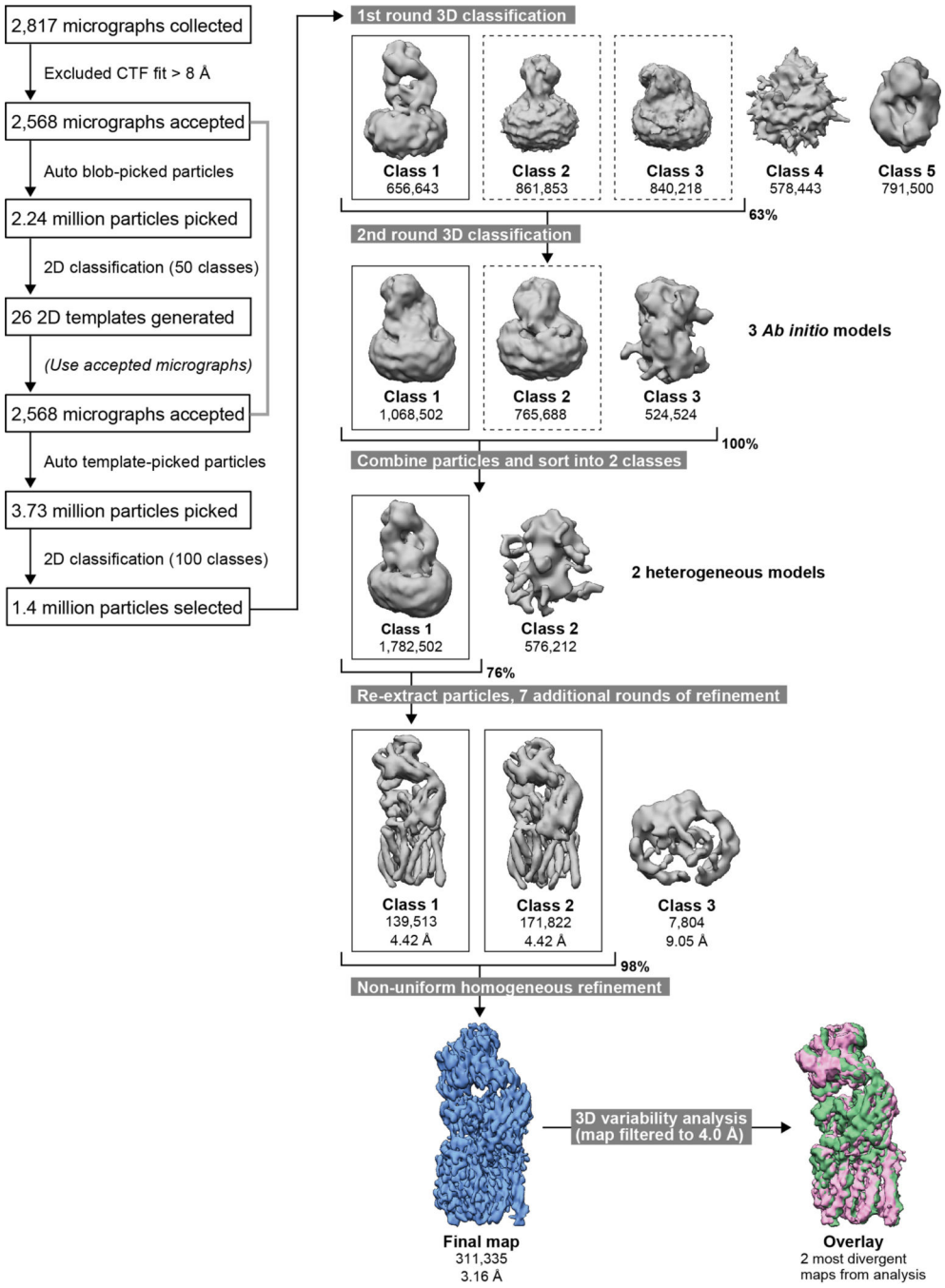

Extended Data Fig. 2. Workflow for NorA-Fab36 complex structure determination by cryo-EM.
Key steps in cryo-EM data processing are displayed for determination of the coulomb potential map of the NorA-Fab36 complex. Solid and dotted boxes around classes correspond to the intact NorA-Fab36 complex and a NorA-Fab36 complex apparently lacking the constant Fab region, respectively. Underneath each class is the number of particles constituting that class. The percentages in the figure indicate the percentage of particles selected for the subsequent refinement step from the total number of particles

initially inputted into the refinement step. An identical strategy was used for processing images of the NorA-Fab25 complex.

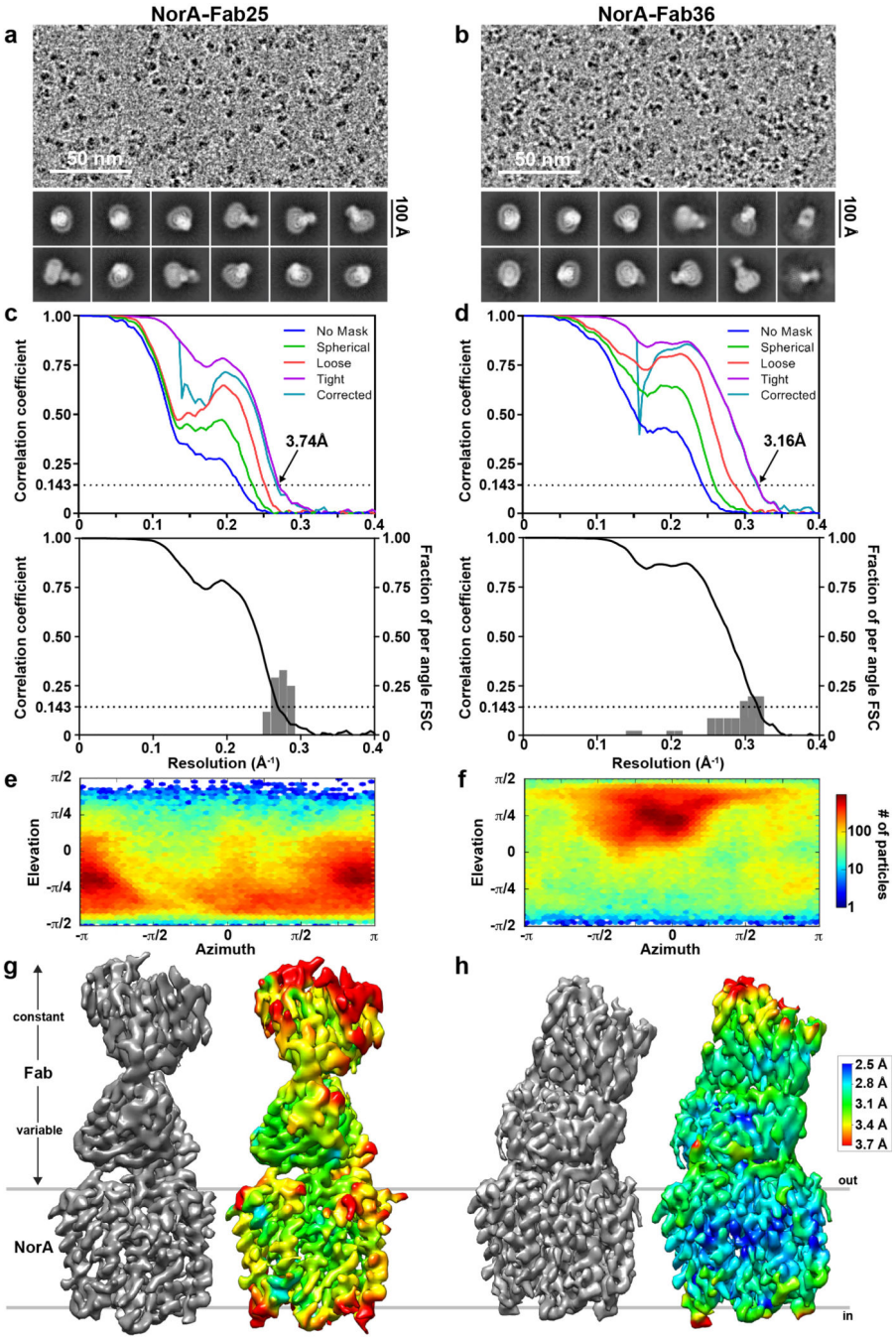

Extended Data Fig. 3. Cryo-EM structure determination of NorA-Fab25 and NorA-Fab36 complexes.

a, b. Representative cryo-EM micrographs (top) and exemplary 2D class averages (bottom) for NorA-Fab25 (a) and NorA-Fab36 (b) complexes. Images were acquired on a 300 kV Krios microscope. The most populous 2D classes show intact NorA-Fab complexes in different orientations.

c, d. Fourier shell correlation (top) and directional FSC (bottom) curves measured for the final NorA-Fab25 (c) and NorA-Fab36 (d) reconstructions. The gold standard resolution (FSC = 0.143) is indicated by an arrow. Histograms within the directional FSC plots (bottom) correspond to the y-axis on the right.

e, f. Orientation distribution heatmaps for the final NorA-Fab25 (e) and NorA-Fab36 (f) reconstructions.

g, h. Coulomb potential maps (left) and local resolution maps (right) of NorA-Fab25 (g) and NorA-Fab36 (h). The local resolution maps are illustrated with the same linear coloring scale, where blue corresponds to regions of higher resolution and red corresponds to regions of lower resolution.

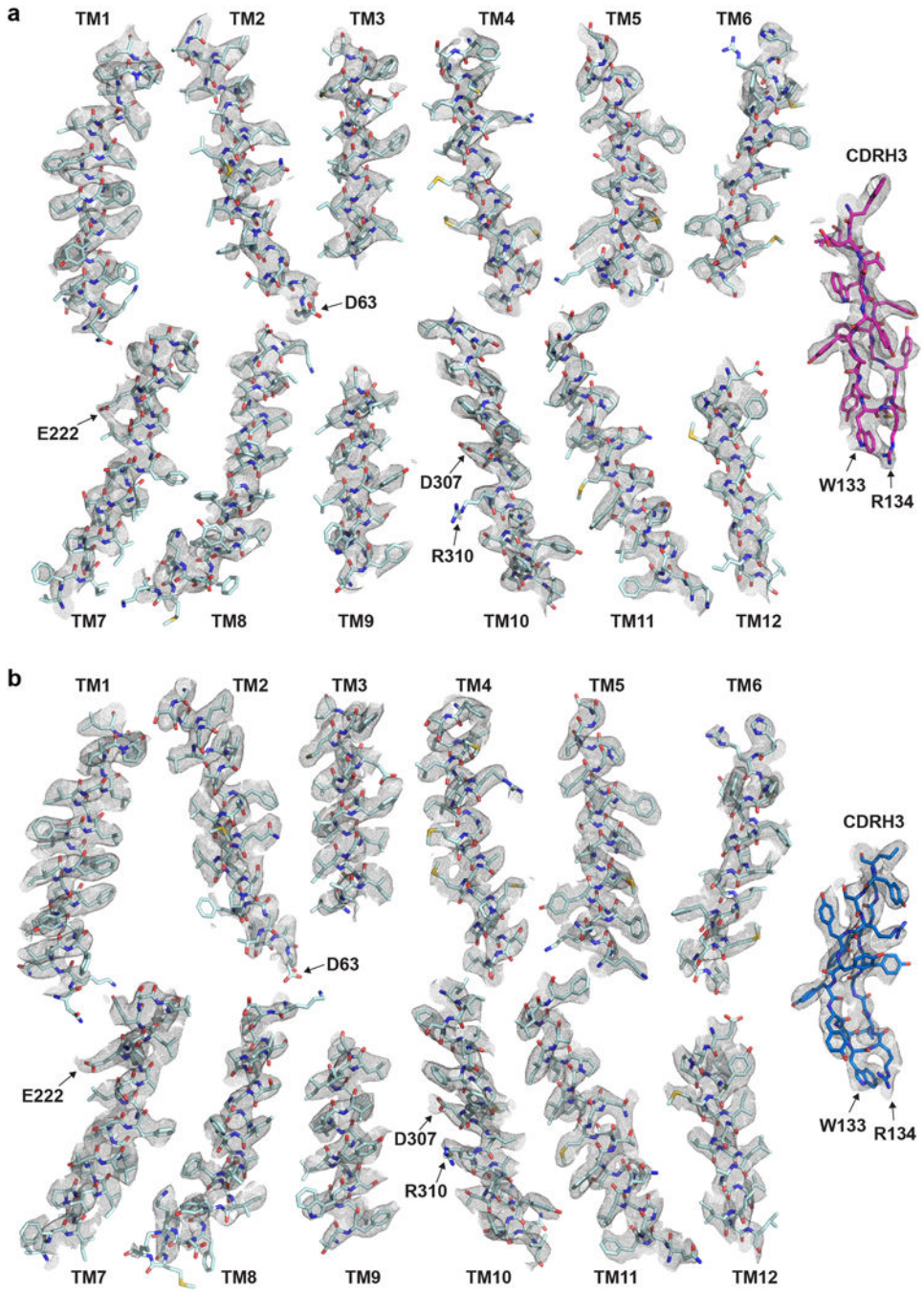

Extended Data Fig. 4. Quality assessment of model-to-map fitting for the NorA-Fab complexes.

a, b. The quality of the NorA-Fab25 (a) and NorA-Fab36 (b) models are illustrated by their respective fit into the experimental maps (shown in mesh). The model-to-map fitting is shown for each TM helix in NorA and a portion of the CDRH3 loop from each Fab. The map contour level was set to 10 sigma units for each TM helix and CDRH3 loop using the *isomesh* command in PyMOL. The following residues comprise each TM domain: TM1, 2–26; TM2, 37–63; TM3, 69–87; TM4, 91–115; TM5, 125–148; TM6, 155–175; TM7, 203–228; TM8, 238–264; TM9, 270–287; TM10, 297–320; TM11, 325–351; TM12, 356–374.

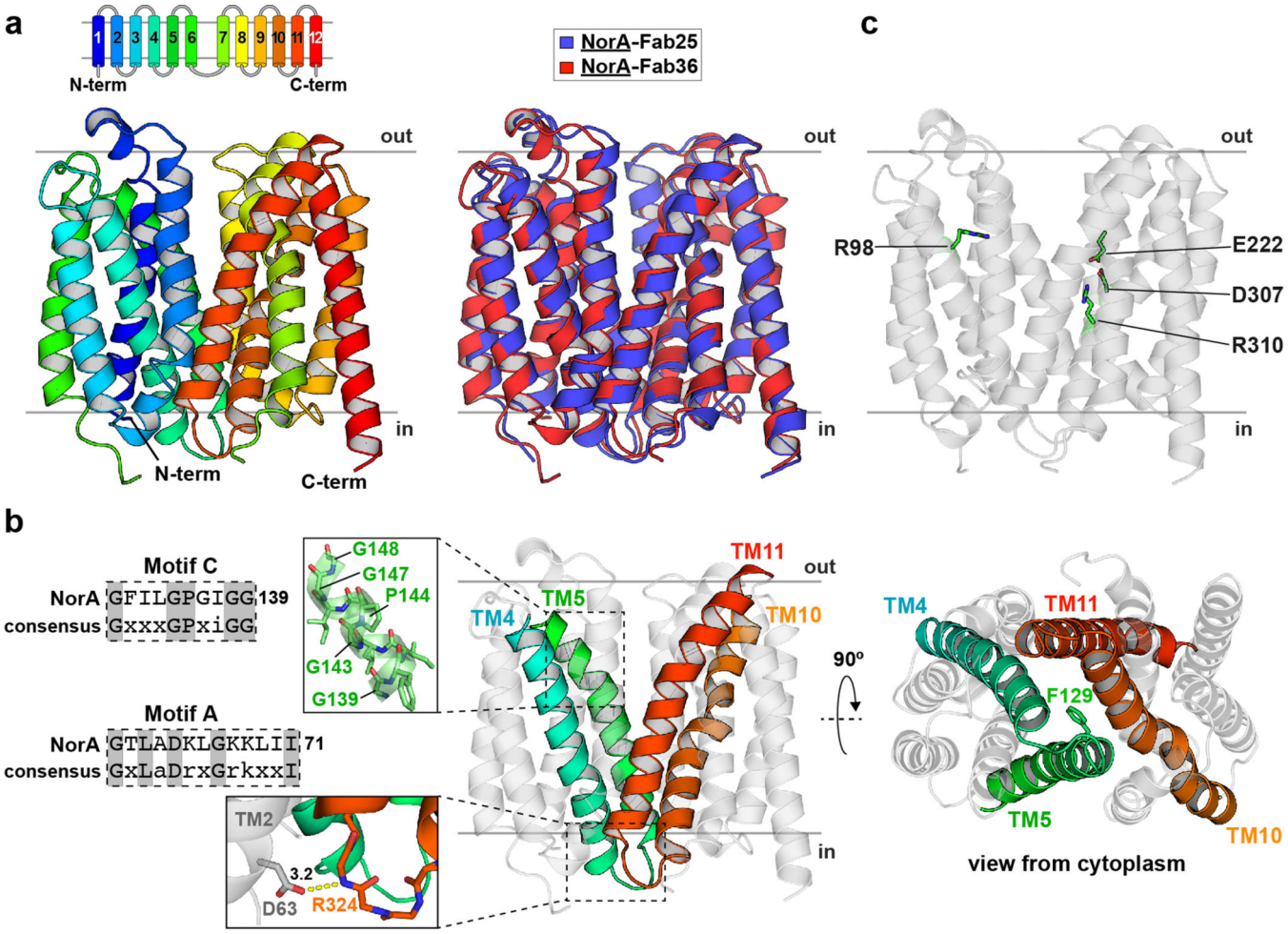

Extended Data Fig. 5. NorA topology and structure.

a. Left: Structure of NorA from the NorA-Fab36 complex where the colors correspond to the 12-TM helices of NorA, as depicted in the cartoon atop the structure. Right: Superimposition of NorA from the NorA-Fab25 structure (blue) with NorA from the NorA-Fab36 structure (red). The all-atom RMSD is 1.2 Å and the C_α RMSD is 0.9 Å.

b. Structural views of NorA from the NorA-Fab36 complex. Left: Sequence alignment of NorA with the consensus sequences for Motif A and Motif C in MFS proteins[8,26]. Identical residues are shaded in grey and lowercase residue codes correspond to less conserved sites than the uppercase residue codes. Middle: Structure of NorA with insets showing expanded views from a portion of Motif A and all of Motif C. The distance (in Å) between the carboxyl side chain of Asp63 (TM2) and the backbone amide of Arg324 (TM11) is shown with a yellow dotted line. Middle, Right: TM4 (cyan), TM5 (green), TM10 (orange), and TM11 (red) seal the substrate binding pocket by forming interhelical contacts on the cytoplasmic side of the membrane. Phe129 from TM5 helps seal the substrate pocket by forming a plug in the middle of these TM helices.

c. Cartoon representation of NorA from the NorA-Fab36 structure displaying the four ionizable residues (green sticks) within the substrate binding pocket: Arg98 (TM4), Glu222 (TM7), Asp307 (TM10), and Arg310 (TM10).

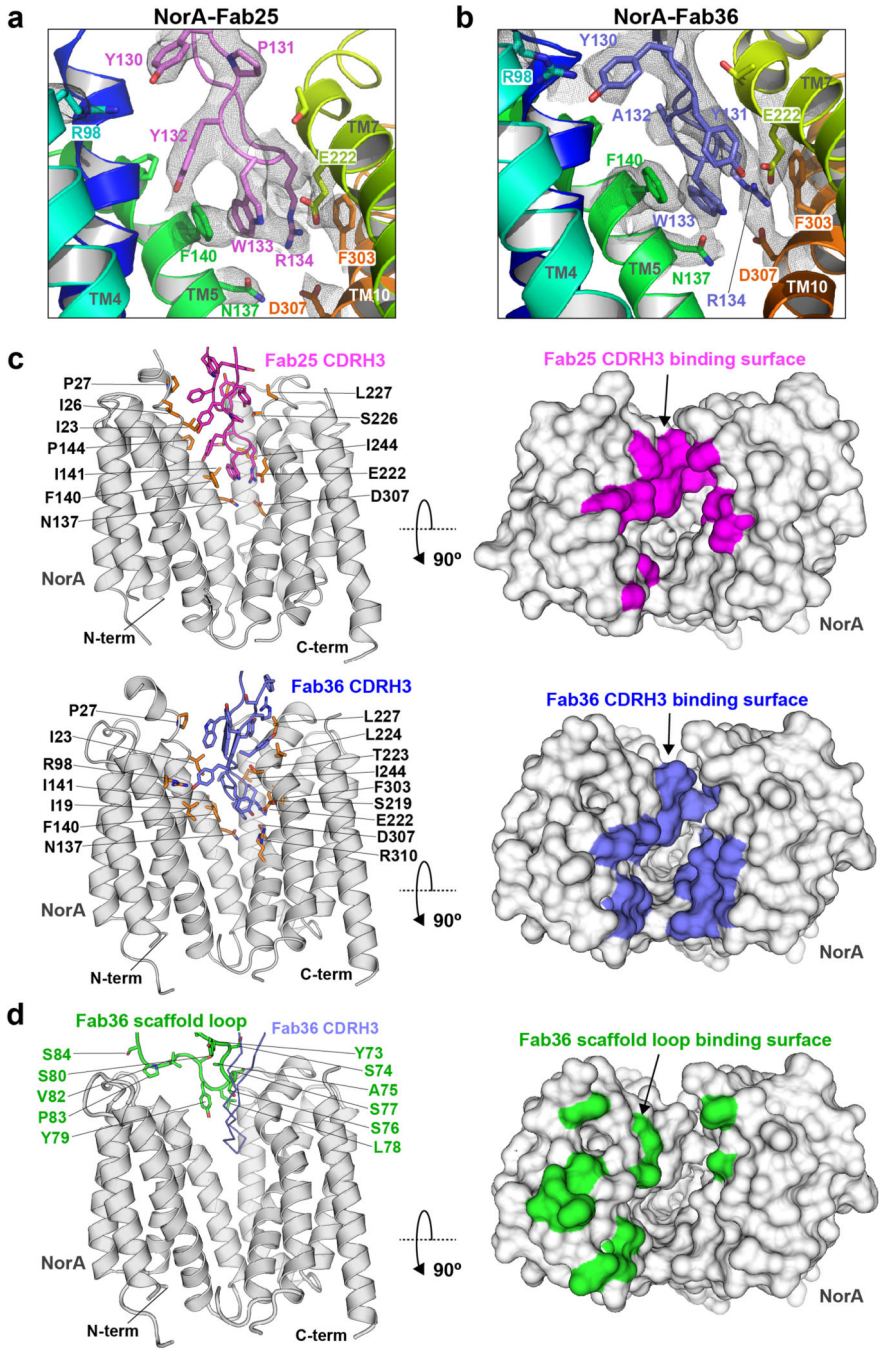

Extended Data Fig. 6. NorA-Fab binding interfaces.

a, b. Detailed views of CDRH3 interactions in the substrate binding pocket of NorA (rainbow) for Fab25 (panel (a); pink) and Fab36 (panel (b); blue). The cryo-EM maps for CDRH3 and select residues of NorA are superimposed on the structural views (grey mesh). **c.** Left: NorA (grey) interacting with CDRH3 from Fab25 (top; magenta) and Fab36 (bottom; blue). NorA residues within 4 Å of CDRH3 residues are labeled and displayed in a stick representation (orange). TM2 and TM11 within NorA are hidden for clarity. Right: View from the outward-facing direction and orthogonal to the membrane surface. NorA

(grey) is shown in a surface representation with the magenta and blue colors indicating NorA residues within 4 Å of Fab25 CDRH3 or Fab36 CDRH3, respectively. Fab25 and Fab36 are not shown for clarity.

d. Left: NorA (grey) interacting with an elongated loop on Fab36 with select residues displayed in stick representation (green). This loop is formed by scaffold residues Leu71 to Arg85 of the Fab light chain variable domain. The CDRH3 loop is shown in ribbon (light blue). TM2 and TM11 within NorA are hidden for clarity. Right: View from the outward-facing direction and orthogonal to the membrane surface. NorA (grey) is shown in a surface representation with the green color indicating NorA residues within 4 Å of the Fab36 light chain scaffold loop. Fab36 is not shown for clarity.

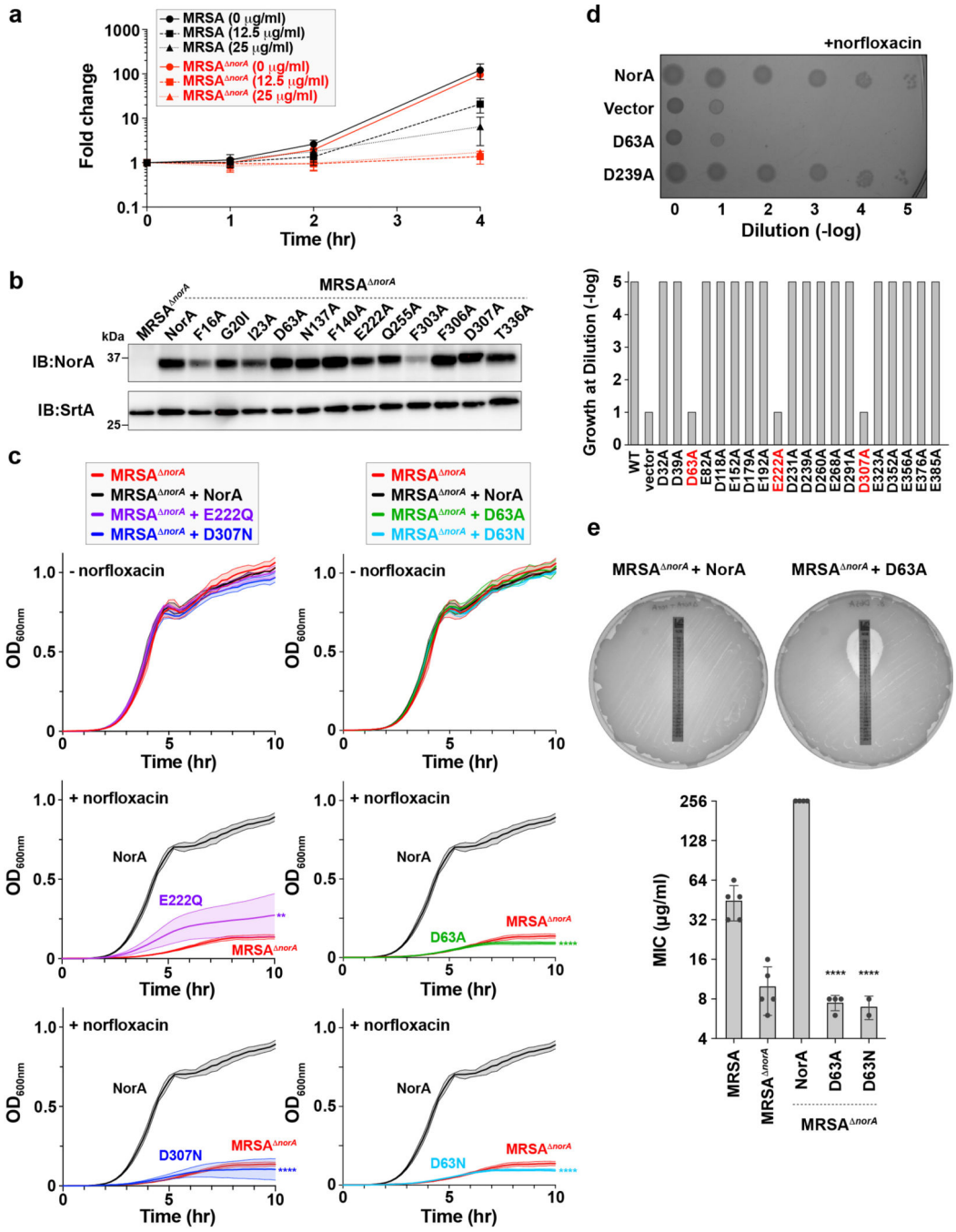

Extended Data Fig. 7. Expression and function of NorA mutants in MRSA and *E. coli*.

a. Dilution experiment in MRSA and MRSA$^{\Delta norA}$ strains to test bacteriostatic or bactericidal effect of norfloxacin. Cells were grown overnight to saturation, diluted 1,000-fold into fresh media containing norfloxacin at 0, 12.5, or 25 μg/ml, grown in liquid culture for 1, 2, or 4 hr, and plated on solid media for determination of colony forming units (CFUs). The fold change refers to CFUs at the 1, 2, and 4 hr time points relative to Time = 0 hr, which did not contain norfloxacin. Data are presented as mean values +/− s.d. among three replicates.

b. Immunoblot analysis of the membrane fraction after induction of MRSA$^{\Delta norA}$ or MRSA$^{\Delta norA}$ transformed with a hemin-inducible plasmid encoding wild-type NorA and NorA mutants. The samples were immunoblotted for NorA and SrtA (control membrane protein). Similar results were obtained in two immunoblots.

c. Growth inhibition experiments using the MRSA$^{\Delta norA}$ strain transformed with a hemin-inducible plasmid encoding NorA or NorA mutants. NorA expression was induced with 1 μM hemin and carried out in the presence or absence of 12.5 μg/mL norfloxacin. Solid lines and shading in the same color correspond to the average and standard deviation of four technical replicates from one representative experiment, respectively. Similar results were verified in at least two independent experiments. P-values were calculated using an unpaired, two-tailed t-test for each single-site mutant relative to MRSA$^{\Delta norA}$ + NorA at the 10 hr timepoint: **** $P<0.0001$, ** $P=0.0045$.

d. Top: Representative serial dilution experiment on LB agar using *E. coli* transformed with a plasmid encoding NorA or NorA mutants in the presence of norfloxacin (15 nM). Bottom: Results of serial dilution experiments for 20 single-site NorA mutants at aspartate and glutamate positions. Three mutants showed ablated resistance phenotypes toward norfloxacin (D63A, E222A, and D307A). The serial dilution screen was performed one time; loss-of-function mutants identified from the screen were confirmed in independent *E. coli* serial dilution experiments and in MRSA$^{\Delta norA}$ using MIC and growth inhibition experiments.

e. Top: Representative images from norfloxacin MIC experiments using MRSA$^{\Delta norA}$ strains transformed with a hemin-inducible plasmid encoding NorA (left) or D63A (right). NorA expression was induced with 1 μM hemin. The MIC values were read at the intersection of the inhibition eclipse and the strip (units of μg/ml). Bottom: Plot of norfloxacin MIC values for MRSA or MRSA$^{\Delta norA}$ transformed with plasmids encoding wild-type NorA or NorA mutants. The MIC upper limit of detection was 256 μg/ml. P-values were calculated using an unpaired, two-tailed t-test for each single-site mutant relative to MRSA$^{\Delta norA}$ + NorA: **** $P<0.0001$. The number of independent MIC experiments (n=2–5) correspond to the number of black circles superimposed on the bar graph for each sample; data are presented as mean values +/− s.d. among the independent experiments.

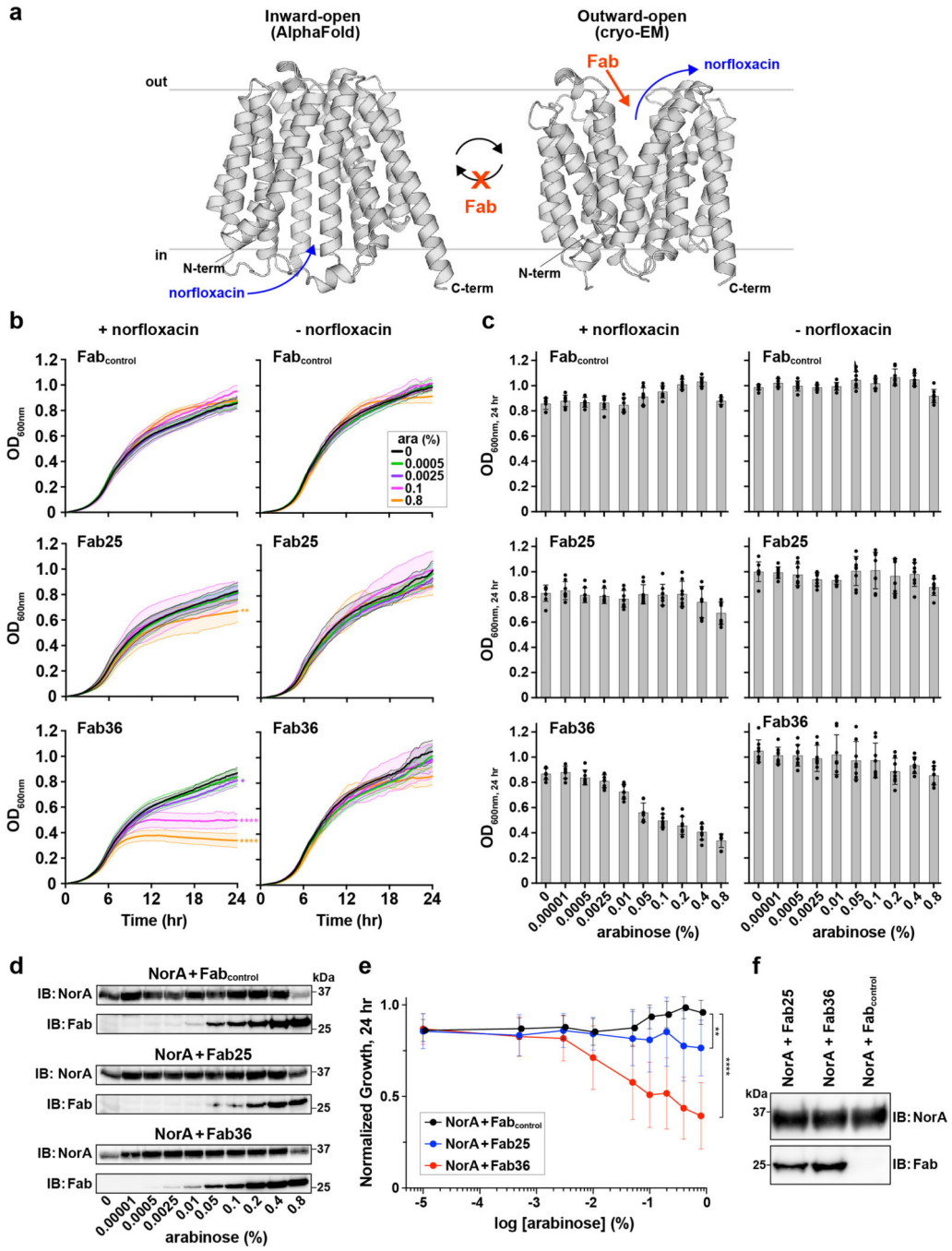

Extended Data Fig. 8. Fab inhibition of NorA assessed through an *E. coli* co-expression assay.

a. Schematic illustrating Fab inhibition of NorA-mediated norfloxacin efflux. The AlphaFold model of inward-open NorA[60] is shown on the left and the cryo-EM structure of outward-open NorA from the NorA-Fab36 complex is displayed on the right. Efflux of norfloxacin is mediated by NorA in the absence of Fab (black arrow), whereas efflux is inhibited when NorA is bound to Fab (red "X").

b. Growth inhibition experiment of *E. coli* co-expressing NorA and $Fab_{control}$, Fab25, or Fab36. Experiments were performed in the presence (left) or absence (right) of 1.2 μg/mL

norfloxacin and arabinose (inducer of Fabs; abbreviated “ara”). For clarity, only a few datasets at select arabinose concentrations are displayed. Solid lines and shading in the same color correspond to the average and standard deviation of four independent experiments, respectively. P-values were calculated using an unpaired, two-tailed t-test with Welch’s correction for the 24 hr timepoint and indicate significance relative to the 0% arabinose concentration: **** P<0.0001, ** P=0.0013, * P=0.0305.

c. Analysis of the growth inhibition data at the 24 hr timepoint for *E. coli* co-expressing NorA and $Fab_{control}$, Fab25, or Fab36 as a function of arabinose concentration. Bar graphs indicate the average and standard deviation among four independent experiments, each with two replicates per experiment. Black circles correspond to all replicate datapoints from the independent experiments.

d. Immunoblot analyses of *E. coli* co-expressing NorA and $Fab_{control}$, Fab25, or Fab36 after 24 hr of growth and in the presence of varying arabinose concentration. Analyses were performed from growths in the absence of norfloxacin to normalize against growth inhibition variation when norfloxacin was present. Similar results were obtained in two immunoblots.

e. Normalized *E. coli* growth curves calculated by dividing the $OD_{600nm,\ 24\ hr}$ value in the presence of norfloxacin by the corresponding value in the absence of norfloxacin for each arabinose concentration. Data are presented as mean values +/− s.d. among four independent experiments. P-values were calculated using an unpaired, two-tailed t-test with Welch’s correction for the highest arabinose concentration for the NorA + Fab25 and NorA + Fab36 samples relative to the NorA + $Fab_{control}$ sample: **** P<0.0001, ** P=0.0084.

f. Immunoblot analysis of a NorA pull-down experiment for *E. coli* co-expressing NorA and $Fab_{control}$, Fab25, or Fab36 with 0.2% arabinose. Following co-expression, cells were lysed and NorA was purified from the membrane fraction using affinity chromatography. Elution fractions were immunoblotted for NorA and Fab. Similar results were obtained in two immunoblots.

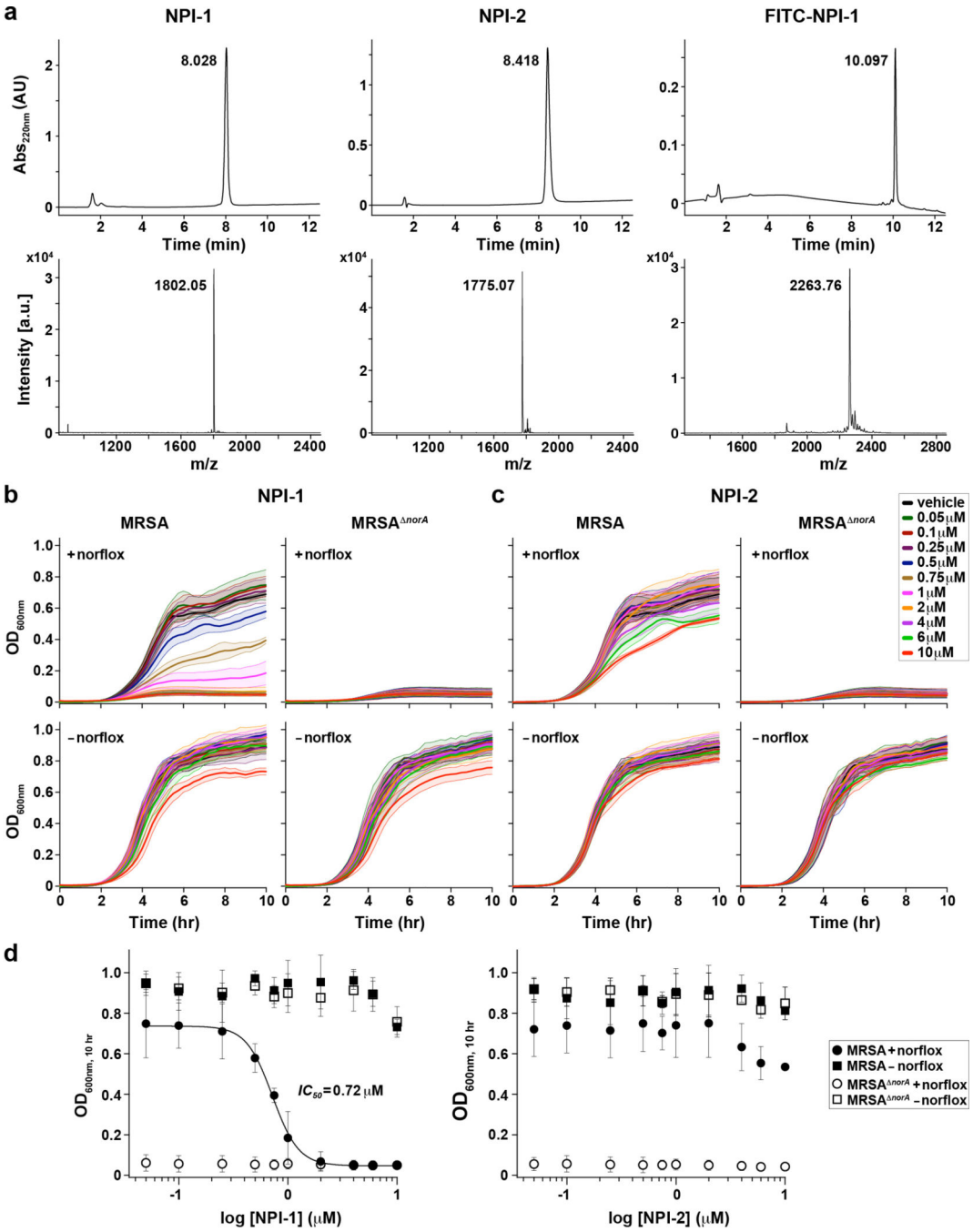

Extended Data Fig. 9. Inhibition of MRSA growth by combination treatment of norfloxacin and a CDRH3 mimicking peptide targeting NorA.

a. Analytical HPLC traces (top row) and MALDI-TOF (bottom row) of purified NPI-1, NPI-2, and FITC-NPI-1 peptides. NPI-1: observed mass of 1802.05 $[M+H]^+$; calculated mass of 1801.85 $[M+H]^+$. NPI-2: observed mass of 1775.07 $[M+H]^+$; calculated mass of 1774.79 $[M+H]^+$. FITC-NPI-1: observed mass of 2263.76 $[M+H]^+$; calculated mass of 2263.95 $[M+H]^+$.

b, c. Growth inhibition of MRSA or MRSA$^{\Delta norA}$ treated with varying concentrations of (b) NPI-1 or (c) NPI-2 in the presence or absence of norfloxacin (12.5 μg/ml). The peptide was added at the start of the time course (Time = 0 hr). Solid lines and shading in the same color correspond to the average and standard deviation of three independent experiments, respectively.

d. Growth inhibition of MRSA or MRSA$^{\Delta norA}$ at the 10 hr timepoint from (b) and (c) plotted against the NPI-1 (left) or NPI-2 (right) concentration, respectively. Data are presented as mean values +/− s.d. among three independent experiments. The fitted curve was used to determine the IC_{50} for NPI-1 (0.72 ± 0.08 μM).

Supplementary Material

Refer to Web version on PubMed Central for supplementary material.

Acknowledgements

This work was supported by NIH (R01AI165782, R01AI108889) and NSF awards (MCB 1902449) to N.J.T., NIH awards (R01AI165782, R01NS108151, R01GM121994, R01DK099023) to D.N.W., NIH awards (R01AI099394, R01AI105129, R01AI137336, R01AI140754, R21AI149350) to V.J.T., NIH award (R01AI165782) to S.K., and NIH award (R35GM130333) to P.S.A. V.J.T. is a Burroughs Wellcome Fund Investigator in the pathogenesis of infectious diseases. D.N.B. was supported by an NIH Predoctoral Training Grant (T32-GM088118). D.B.S. was supported by the American Cancer Society Postdoctoral Fellowship (129844-PF-17–135-01-TBE) and Department of Defense Horizon Award (W81XWH-16–1-0153). We thank D.C. Hooper for sharing a NorA construct in the pTrcHis2C vector and J.F. Hunt for the MSP1E3D1-T277C construct. We thank S. Wang for assistance in optimizing computational resources for cryo-EM data processing at the NYU HPC, M. (Leninger) Crames and A. Tumati for initial NorA experiments that identified LMNG as a suitable solubilizing detergent, P. Tate for assistance in cloning, and I. Irnov, N.K. Karpowich, J.J. Marden, and W.J. Rice for helpful discussions. Negative stain and cryo-EM grids were screened at the Microscopy Facility and the Cryo-Electron Microscopy Facility of the NYU School of Medicine. We thank the Pacific Northwest Cryo-EM Center (PNCC) and laboratory personnel where the large cryo-EM datasets used in the structure determination were collected. EM data processing used computing resources at the HPC facilities of NYU School of Medicine and NYU. The following reagent was provided by the Network on Antimicrobial Resistance in *Staphylococcus aureus* (NARSA) for distribution by BEI Resources, NIAID, NIH: *Staphylococcus aureus* subsp. aureus, Strain JE2, Transposon Mutant NE1034 (SAUSA300_0680), NR-47577. The pBAD33-Gm vector was obtained through Addgene (plasmid #65098; http://n2t.net/addgene:65098; RRID:Addgene_65098).

References

1. CDC. Antibiotic Resistance Threats in the United States. U.S. Department of Health and Human Services., (10.15620/cdc:82532, Atlanta, GA, 2019).
2. Nikaido H Multidrug resistance in bacteria. Annu Rev Biochem 78, 119–146 (2009). [PubMed: 19231985]
3. Du D et al. Multidrug efflux pumps: structure, function and regulation. Nat Rev Microbiol 16, 523–539 (2018). [PubMed: 30002505]
4. Piddock LJ Multidrug-resistance efflux pumps - not just for resistance. Nat Rev Microbiol 4, 629–636 (2006). [PubMed: 16845433]
5. Singh R et al. Temporal Interplay between Efflux Pumps and Target Mutations in Development of Antibiotic Resistance in *Escherichia coli*. Antimicrob Agents Chemother 56, 1680–1685 (2012). [PubMed: 22232279]
6. Papkou A, Hedge J, Kapel N, Young B & MacLean RC Efflux pump activity potentiates the evolution of antibiotic resistance across *S. aureus* isolates. Nat Commun 11, 3970 (2020). [PubMed: 32769975]
7. Costa SS et al. Genetic Diversity of norA, Coding for a Main Efflux Pump of Staphylococcus aureus. Front Genet 9, 710 (2018). [PubMed: 30687388]

8. Paulsen IT, Brown MH & Skurray RA Proton-dependent multidrug efflux systems. Microbiol Rev 60, 575–608 (1996). [PubMed: 8987357]
9. Yu JL, Grinius L & Hooper DC NorA functions as a multidrug efflux protein in both cytoplasmic membrane vesicles and reconstituted proteoliposomes. J Bacteriol 184, 1370–1377 (2002). [PubMed: 11844766]
10. Ng EY, Trucksis M & Hooper DC Quinolone resistance mediated by norA: physiologic characterization and relationship to flqB, a quinolone resistance locus on the *Staphylococcus aureus* chromosome. Antimicrob Agents Chemother 38, 1345–1355 (1994). [PubMed: 8092836]
11. Kaatz GW, Thyagarajan RV & Seo SM Effect of promoter region mutations and mgrA overexpression on transcription of norA, which encodes a *Staphylococcus aureus* multidrug efflux transporter. Antimicrob Agents Chemother 49, 161–169 (2005). [PubMed: 15616291]
12. DeMarco CE et al. Efflux-related resistance to norfloxacin, dyes, and biocides in bloodstream isolates of *Staphylococcus aureus*. Antimicrob Agents Chemother 51, 3235–3239 (2007). [PubMed: 17576828]
13. Yoshida H, Bogaki M, Nakamura S, Ubukata K & Konno M Nucleotide sequence and characterization of the *Staphylococcus aureus* norA gene, which confers resistance to quinolones. J Bacteriol 172, 6942–6949 (1990). [PubMed: 2174864]
14. Neyfakh AA, Borsch CM & Kaatz GW Fluoroquinolone resistance protein NorA of *Staphylococcus aureus* is a multidrug efflux transporter. Antimicrob Agents Chemother 37, 128–129 (1993). [PubMed: 8431010]
15. Kaatz GW, Seo SM & Ruble CA Efflux-mediated fluoroquinolone resistance in *Staphylococcus aureus*. Antimicrob Agents Chemother 37, 1086–1094 (1993). [PubMed: 8517696]
16. de Sousa Andrade LM et al. Antimicrobial activity and inhibition of the NorA efflux pump of *Staphylococcus aureus* by extract and isolated compounds from *Arrabidaea brachypoda*. Microb Pathog 140, 103935 (2020).
17. Brincat JP et al. Discovery of novel inhibitors of the NorA multidrug transporter of *Staphylococcus aureus*. J. Med. Chem. 54, 354–365 (2011). [PubMed: 21141825]
18. Kathawala RJ, Gupta P, Ashby CR Jr. & Chen ZS The modulation of ABC transporter-mediated multidrug resistance in cancer: a review of the past decade. Drug Resist Updat 18, 1–17 (2015). [PubMed: 25554624]
19. Renau TE et al. Conformationally-restricted analogues of efflux pump inhibitors that potentiate the activity of levofloxacin in *Pseudomonas aeruginosa*. Bioorg. Med. Chem. Lett. 13, 2755–2758 (2003). [PubMed: 12873508]
20. Sidhu SS & Koide S Phage display for engineering and analyzing protein interaction interfaces. Curr Opin Struct Biol 17, 481–487 (2007). [PubMed: 17870470]
21. Nygaard R, Kim J & Mancia F Cryo-electron microscopy analysis of small membrane proteins. Curr Opin Struct Biol 64, 26–33 (2020). [PubMed: 32603877]
22. Wu S et al. Fabs enable single particle cryoEM studies of small proteins. Structure 20, 582–592 (2012). [PubMed: 22483106]
23. Huang Y, Lemieux MJ, Song J, Auer M & Wang DN Structure and mechanism of the glycerol-3-phosphate transporter from *Escherichia coli*. Science 301, 616–620 (2003). [PubMed: 12893936]
24. Abramson J et al. Structure and mechanism of the lactose permease of *Escherichia coli*. Science 301, 610–615 (2003). [PubMed: 12893935]
25. Law CJ, Maloney PC & Wang DN Ins and outs of major facilitator superfamily antiporters. Annu Rev Microbiol 62, 289–305 (2008). [PubMed: 18537473]
26. Paulsen IT & Skurray RA Topology, structure and evolution of two families of proteins involved in antibiotic and antiseptic resistance in eukaryotes and prokaryotes--an analysis. Gene 124, 1–11 (1993). [PubMed: 8440470]
27. Jiang D et al. Structure of the YajR transporter suggests a transport mechanism based on the conserved motif A. Proc Natl Acad Sci U S A 110, 14664–14669 (2013).
28. Ginn SL, Brown MH & Skurray RA The TetA(K) tetracycline/H(+) antiporter from Staphylococcus aureus: mutagenesis and functional analysis of motif C. J Bacteriol 182, 1492–1498 (2000). [PubMed: 10692352]

29. Klyachko KA, Schuldiner S & Neyfakh AA Mutations affecting substrate specificity of the *Bacillus subtilis* multidrug transporter Bmr. J Bacteriol 179, 2189–2193 (1997). [PubMed: 9079903]
30. Fey PD et al. A genetic resource for rapid and comprehensive phenotype screening of nonessential Staphylococcus aureus genes. Mbio 4, e00537–00512 (2013).
31. Torres VJ et al. A *Staphylococcus aureus* regulatory system that responds to host heme and modulates virulence. Cell Host Microbe 1, 109–119 (2007). [PubMed: 18005689]
32. Schuldiner S Competition as a way of life for H(+)-coupled antiporters. J Mol Biol 426, 2539–2546 (2014). [PubMed: 24862284]
33. Yin Y, He X, Szewczyk P, Nguyen T & Chang G Structure of the multidrug transporter EmrD from *Escherichia coli*. Science 312, 741–744 (2006). [PubMed: 16675700]
34. Debruycker V et al. An embedded lipid in the multidrug transporter LmrP suggests a mechanism for polyspecificity. Nat Struct Mol Biol 27, 829–835 (2020). [PubMed: 32719456]
35. Heng J et al. Substrate-bound structure of the *E. coli* multidrug resistance transporter MdfA. Cell Res 25, 1060–1073 (2015). [PubMed: 26238402]
36. Fluman N, Ryan CM, Whitelegge JP & Bibi E Dissection of mechanistic principles of a secondary multidrug efflux protein. Mol Cell 47, 777–787 (2012). [PubMed: 22841484]
37. Pasquina-Lemonche L et al. The architecture of the Gram-positive bacterial cell wall. Nature 582, 294–297 (2020). [PubMed: 32523118]
38. Sawyer N & Arora PS Hydrogen Bond Surrogate Stabilization of beta-Hairpins. Acs Chem Biol 13, 2027–2032 (2018). [PubMed: 30005156]

Methods References

39. Studier FW Protein production by auto-induction in high density shaking cultures. Protein Expr Purif 41, 207–234 (2005). [PubMed: 15915565]
40. Karpowich NK, Song JM, Cocco N & Wang DN ATP binding drives substrate capture in an ECF transporter by a release-and-catch mechanism. Nat Struct Mol Biol 22, 565–571 (2015). [PubMed: 26052893]
41. Sauer DB et al. Structural basis for the reaction cycle of DASS dicarboxylate transporters. Elife 9, e61350 (2020).
42. Fellouse FA et al. High-throughput generation of synthetic antibodies from highly functional minimalist phage-displayed libraries. J Mol Biol 373, 924–940 (2007). [PubMed: 17825836]
43. Dominik PK & Kossiakoff AA Phage display selections for affinity reagents to membrane proteins in nanodiscs. Methods Enzymol 557, 219–245 (2015). [PubMed: 25950967]
44. Sidhu SS, Lowman HB, Cunningham BC & Wells JA Phage display for selection of novel binding peptides. Methods Enzymol 328, 333–363 (2000). [PubMed: 11075354]
45. Burioni R et al. A vector for the expression of recombinant monoclonal Fab fragments in bacteria. J Immunol Methods 217, 195–199 (1998). [PubMed: 9776589]
46. Bailey LJ et al. Locking the Elbow: Improved Antibody Fab Fragments as Chaperones for Structure Determination. J Mol Biol 430, 337–347 (2018). [PubMed: 29273204]
47. Nikolovska-Coleska Z et al. Development and optimization of a binding assay for the XIAP BIR3 domain using fluorescence polarization. Anal. Biochem. 332, 261–273 (2004). [PubMed: 15325294]
48. Huang XY Fluorescence polarization competition assay: The range of resolvable inhibitor potency is limited by the affinity of the fluorescent ligand. J Biomol Screen 8, 34–38 (2003). [PubMed: 12854996]
49. Sauer DB et al. Structure and inhibition mechanism of the human citrate transporter NaCT. Nature 591, 157–161 (2021). [PubMed: 33597751]
50. Mastronarde DN Automated electron microscope tomography using robust prediction of specimen movements. J Struct Biol 152, 36–51 (2005). [PubMed: 16182563]

51. Punjani A, Rubinstein JL, Fleet DJ & Brubaker MA cryoSPARC: algorithms for rapid unsupervised cryo-EM structure determination. Nat Methods 14, 290–296 (2017). [PubMed: 28165473]
52. Adams PD et al. PHENIX: a comprehensive Python-based system for macromolecular structure solution. Acta Crystallogr D Biol Crystallogr 66, 213–221 (2010). [PubMed: 20124702]
53. Tan YZ et al. Addressing preferred specimen orientation in single-particle cryo-EM through tilting. Nat Methods 14, 793–796 (2017). [PubMed: 28671674]
54. Grant T, Rohou A & Grigorieff N cisTEM, user-friendly software for single-particle image processing. Elife 7 (2018).
55. Dang S et al. Cryo-EM structures of the TMEM16A calcium-activated chloride channel. Nature 552, 426–429 (2017). [PubMed: 29236684]
56. Pettersen EF et al. UCSF Chimera--a visualization system for exploratory research and analysis. J Comput Chem 25, 1605–1612 (2004). [PubMed: 15264254]
57. Emsley P & Cowtan K Coot: model-building tools for molecular graphics. Acta Crystallogr D Biol Crystallogr 60, 2126–2132 (2004). [PubMed: 15572765]
58. Mazmanian SK et al. Passage of heme-iron across the envelope of *Staphylococcus aureus*. Science 299, 906–909 (2003). [PubMed: 12574635]
59. Jimenez N et al. Genetics and proteomics of *Aeromonas salmonicida* lipopolysaccharide core biosynthesis. J Bacteriol 191, 2228–2236 (2009). [PubMed: 19151135]
60. https://alphafold.ebi.ac.uk/entry/Q2G0A2. (Accessed October 4, 2021).

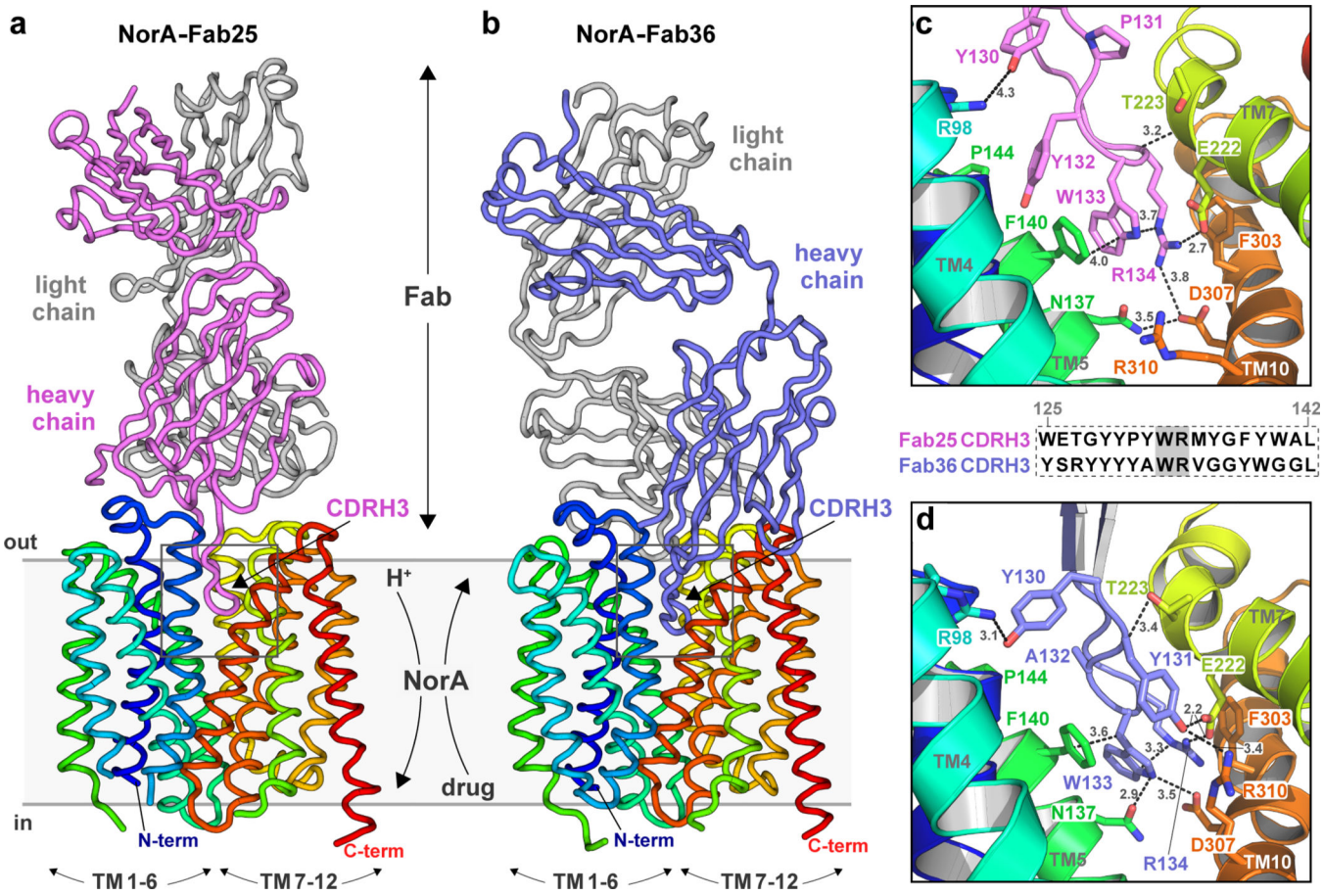

Figure 1. NorA-Fab complex structures determined using single particle cryo-EM.

a, b. NorA structures were solved in complex with Fab25 at 3.74 Å (a) and Fab36 at 3.16 Å resolution (b) using cryo-EM. The light and heavy chains of Fab25 are shown in grey and pink, while those of Fab36 are shown in grey and light blue, respectively. The transmembrane helices of NorA are colored in rainbow. TM1–6 and TM7–12 define the N- and C-domains of the transporter, respectively.

c, d. Expanded views of CDRH3 interactions for Fab25 (c) and Fab36 (d) in the substrate binding pocket of NorA. Distances (in Å) are displayed as dotted black lines. The primary sequences of CDRH3 for Fab25 and Fab36 are shown between the panels with the tryptophan-arginine motif highlighted in grey.

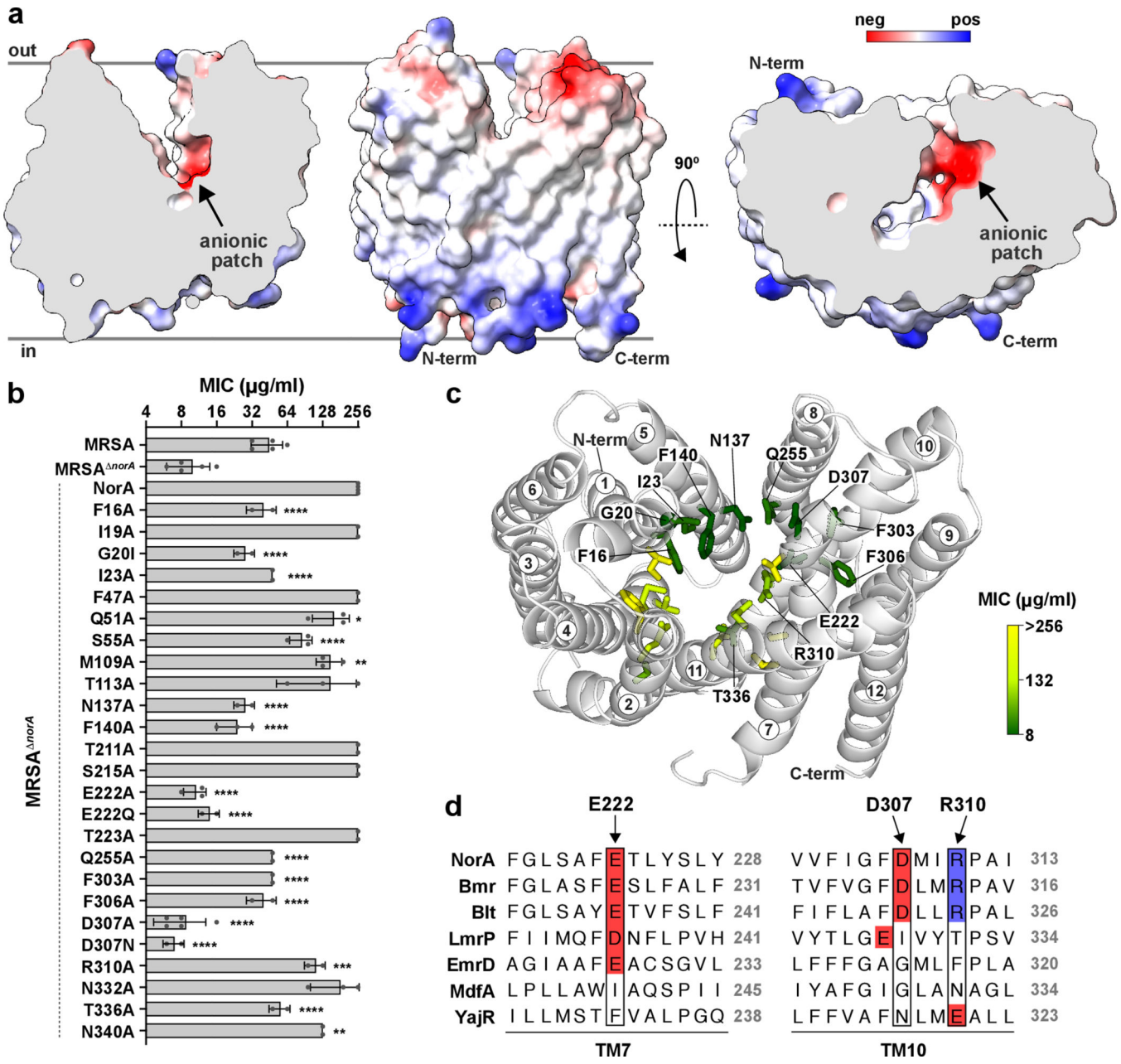

Figure 2. Identification of key residues within NorA essential for drug resistance.

a. Electrostatic surface representations of NorA, where red and blue colors correspond to negatively and positively charged sites, respectively. The left and middle views are depicted in a similar orientation as Fig. 1a, b. The left and right panels display slices of the binding pocket illustrating the anionic patch formed by Glu222 and Asp307. The right panel is rotated by 90° relative to the left and center panels and depicts NorA from the extracellular side of the membrane, looking into the outward-open substrate binding pocket.

b. Norfloxacin MIC values in MRSA obtained for the wild-type strain (MRSA) or a strain with the native NorA gene disrupted by a transposon insertion (MRSA$^{\Delta norA}$). NorA mutants denoted under the MRSA$^{\Delta norA}$ dotted line were expressed from a hemin-inducible plasmid,

where NorA corresponds to the wild-type sequence. The number of independent MIC experiments (n=2–5) corresponds to the number of grey circles superimposed on the bar graph for each sample; data are presented as mean values +/− s.d. among the independent experiments. The MIC upper limit of detection was 256 μg/ml; mutants with reported MIC values at 256 μg/ml may have a true MIC that exceed this value. P-values were calculated using an unpaired, two-tailed t-test for each single-site mutant relative to MRSA$^{\Delta norA}$ + NorA: **** P<0.0001, *** P<0.001, ** P<0.01, * P=0.0158.

c. MIC values for NorA mutants are displayed on the structure in a heat map representation. NorA is shown in a similar orientation as depicted in the right panel of (a). The heat map follows a linear scale, where green corresponds to loss-of-function and yellow signifies no change in function relative to MRSA$^{\Delta norA}$ + NorA. Circled numbers denote the TM helices of NorA.

d. Sequence homology analysis of seven DHA12-family MFS drug transporters showing a portion of TM7 and TM10, which contain Glu222 and Asp307 in NorA, respectively. Anionic residues are highlighted in red and cationic residues are highlighted in blue.

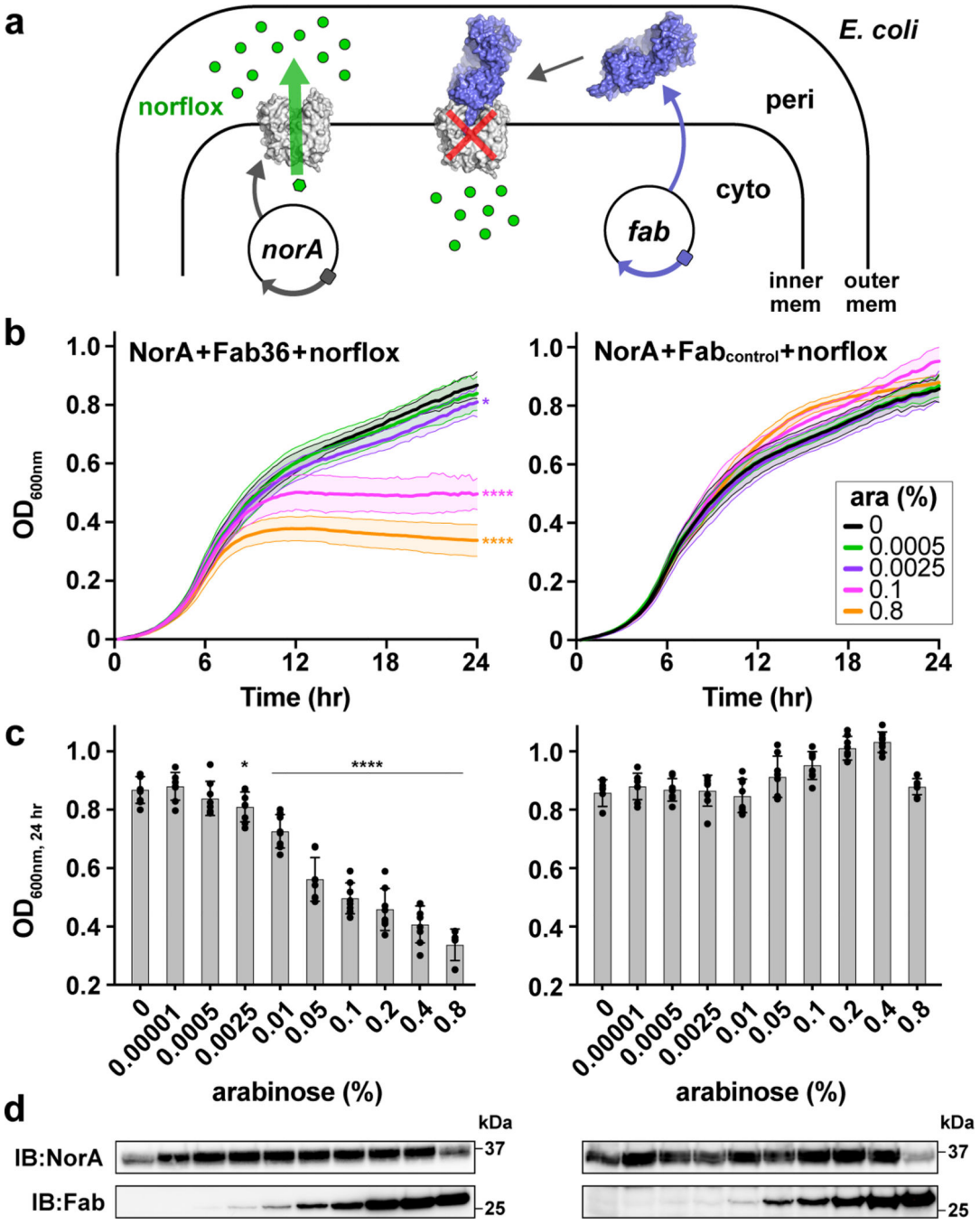

Figure 3. Fab binding and inhibition of NorA.

a. Schematic of *E. coli* co-expression assay involving separate inducible promoters for *norA* and *fab* genes encoded on plasmids (circles). NorA (grey; surface representation) folds in the inner membrane and the Fab (blue; surface representation) is secreted to the periplasm. Efflux of norfloxacin (green circles) is mediated by NorA in the absence of Fab (green arrow), whereas efflux is inhibited when NorA is bound to Fab (red "X").

b. Growth inhibition experiments of *E. coli* co-expressing NorA and Fab36 (left) or $Fab_{control}$ (right) in the presence of norfloxacin and arabinose (inducer of Fabs; abbreviated

"ara"). For clarity, only a few datasets at select arabinose concentrations are displayed. Solid lines and shading in the same color correspond to the average and standard deviation of four independent experiments, respectively, with each independent experiment performed with two technical replicates. P-values were calculated using an unpaired, two-tailed t-test with Welch's correction for the 24 hr timepoint and indicate significance relative to the 0% arabinose concentration: **** $P<0.0001$, * $P=0.0305$.

c. Growth inhibition at the 24 hr timepoint of *E. coli* co-expressing NorA and Fab36 (left) or $Fab_{control}$ (right) as a function of arabinose concentration. Bar graphs indicate the average and standard deviation among four independent experiments. Black circles correspond to all replicate datapoints from the independent experiments. P-values are the same as described in panel (b).

d. Immunoblot (IB) analyses probing for NorA and Fab expression at 24 hr and corresponding to the arabinose concentrations in panel (c). Analyses were performed from growths in the absence of norfloxacin to normalize against growth inhibition variation when norfloxacin was present. Similar results were obtained in two independent experiments.

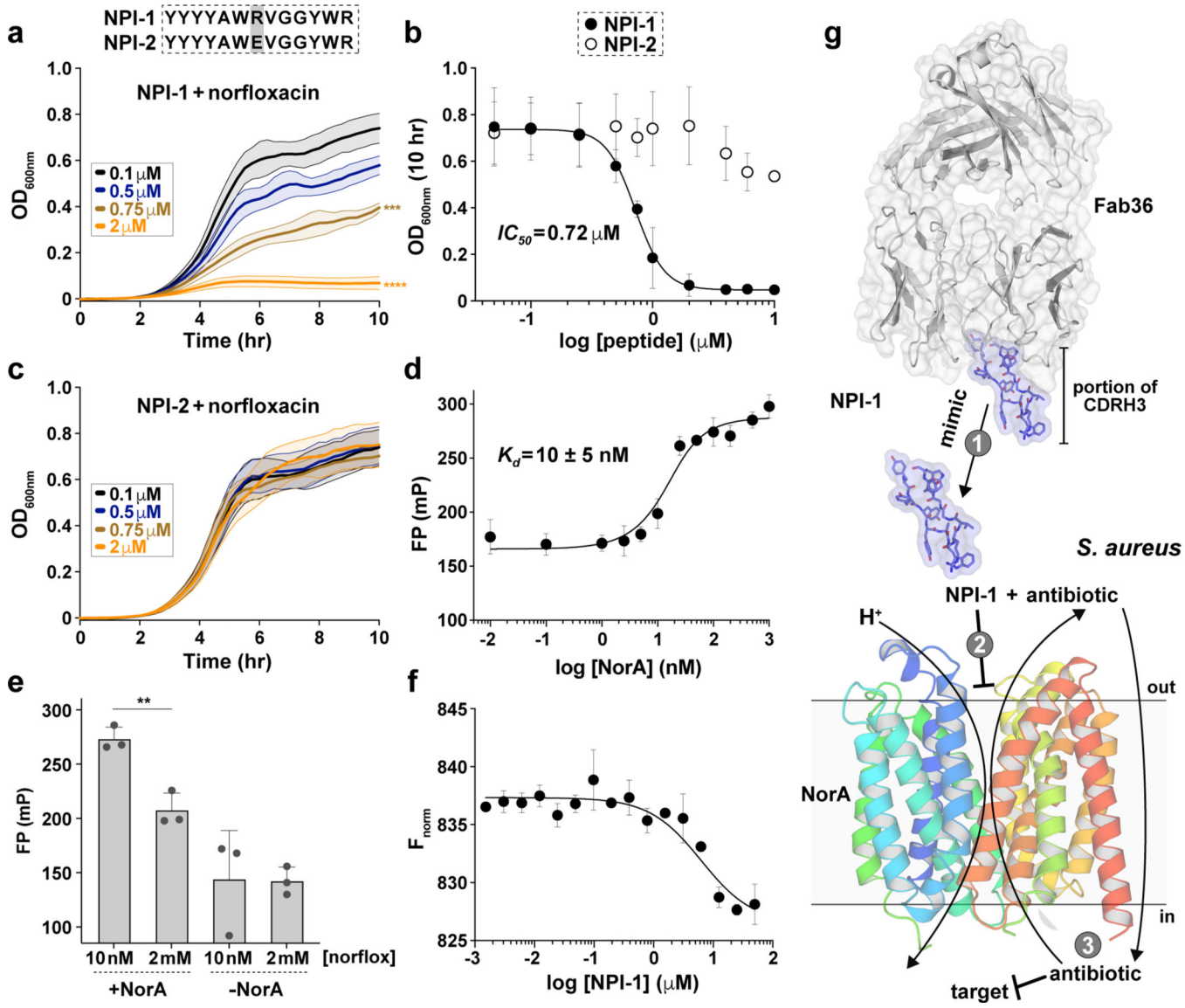

Figure 4. NorA binding and MRSA growth inhibition by a peptide mimicking CDRH3.

a, c. Growth inhibition experiments in MRSA in the presence of norfloxacin (12.5 μg/ml) and varying concentrations of NPI-1 (a) or NPI-2 (c). Solid lines and shading in the same color correspond to the average and standard deviation of three independent experiments, respectively. P-values were calculated using an unpaired, two-tailed t-test for the 10 hr timepoint and indicate significance relative to the vehicle: **** P<0.0001, *** P<0.001.

b. Growth inhibition experiments in MRSA at the 10 hr timepoint as a function of peptide concentration in the presence of 12.5 μg/ml norfloxacin. Data are presented as mean values +/− s.d. among three independent experiments. The fitted curve was used to determine the IC_{50} for NPI-1 (0.72 ± 0.08 μM).

d. Representative fluorescence polarization (FP) experiment using FITC-NPI-1 in the presence of varying NorA concentrations. The solid line reflects the best fit to the data. The reported K_d value and error reflects the average and standard deviation from seven independent experiments.

e. Representative competitive FP binding experiment with a fixed concentrations of NorA and FITC-NPI-1 and a variable concentration of norfloxacin. The control experiment has the same amount of FITC-NPI-1 in the absence of NorA. Three replicate data points in grey circles are superimposed on the bar graph; data are presented as mean values +/− s.d. among the replicates. A P-value was calculated using an unpaired, two-tailed t-test with Welch's correction for the "+NorA" dataset and indicates significance between the two norfloxacin concentrations: ** P=0.006. Similar results were obtained in four independent experiments. **f.** Competitive MST binding experiment with fixed concentrations of NorA and fluorescently labelled Fab36 and a variable concentration of NPI-1. Data are presented as mean values +/− s.d. among three replicates. The line on the plot was calculated using the K_d value determined for FITC-NPI-1 from the FP experiments in panel (d) (see Methods). **g.** Cartoon illustrating the strategy for MRSA growth inhibition through the addition of NPI-1 and antibiotic. The peptide NPI-1 was designed based on the portion of the Fab CDRH3 loop that inserts within the substrate binding pocket of NorA (step 1). When exogenously administered to MRSA, NPI-1 diffuses through the peptidoglycan layer, binds NorA, and inhibits antibiotic efflux (step 2). In turn, this raises the intracellular antibiotic concentration (step 3) and leads to MRSA growth arrest.